OIL DROPLET MANIPULATION ON SUPEROMNIPHOBIC TEXTURED SURFACES

A THESIS SUBMITTED TO

THE GRADUATE SCHOOL OF ENGINEERING AND SCIENCE

OF BILKENT UNIVERSITY

IN PARTIAL FULFULLMENT OF THE REQUIREMENTS FOR

THE DEGREE OF

MASTER OF SCIENCE

IN

MATERIALS SCIENCE AND NANOTECHNOLOGY

By
Ecem Yelekli
July 2020

OIL DROPLET MANIPULATION ON SUPEROMNIPHOBIC TEXTURED SURFACES

By Ecem Yelekli

July 2020

We certify that we have read this thesis and that in our opinion it is fully adequate, in scope and in quality, as a thesis for the degree of Master of Science.

_____

E.Yegan Erdem Ercan (Advisor)

_____

Bilge Baytekin

_____

Ender Yıldırım

Approved for the Graduate School of Engineering and Science:

_____

Ezhan Karaşan
Director of the Graduate School

ABSTRACT

OIL DROPLET MANIPULATION ON SUPEROMNIPHOBIC TEXTURED SURFACES

Ecem Yelekli

M.S in Materials Science and Nanotechnology

Advisor: Asst. Prof. Dr. E. Yegan Erdem Ercan

July, 2020

Microfluidic systems are mostly composed of closed microchannels in which flow is generated by syringe or pressure pumps. The flow in these channels can be droplet-based however access to each droplet individually in these systems is not possible. As an alternative approach to these channel-based devices, droplets can also be manipulated on surfaces by generating surface energy gradients. Since in these systems droplets can be handled individually and samples can be carried in small packages, these systems can perform more controlled operations. For instance, the concentration and volume of the samples can be adjusted more precisely. These systems can be very useful for biological analysis as well as chemical synthesis. Until now, transport of water droplets by using surface energy gradients has been demonstrated in literature. On the other hand, controlled transport of oil droplets on surfaces remained as a challenging task because of their low surface tension. In addition, in the literature, most of the work about oil droplet transportation was carried out in an aqueous environment, and therefore it restricts its potential for applications.

This work demonstrates the transportation of microliter sized oil droplets by utilizing textured superomniphobic surfaces in a controlled way for the first time. By applying vertical vibration to the surface, oil droplets overcome hysteresis and move by following the textured tracks. Superoleophobicity is required to decrease the affinity of oil on the surface so that the motion of droplets can be achieved.

This system has advantages such as the ability to control droplet motion individually by using a single input (vertical vibration) as well as mixing droplets in precise ratios, preventing clogging in channels and cross contamination as well as eliminating the usage of syringe pumps.

In this project, initial focus was on examining the topography effect on superoleophobicity and fabricating superomniphobic surfaces. Surfaces were fabricated on silicon wafers by using conventional lithography technique. In this stage, two different microstructure profile was used on the surfaces: mushroom microstructure and straight sided microstructure. It was observed that mushroom microstructures were required to maintain superoleophobicity. Also, the effect of side length of microstructures, the distance between the microstructures and TiO_2 coating on wettability were investigated. In order to achieve oil droplet transportation, superomniphobic textured surfaces were developed and these surfaces were tested by applying vertical vibration. As a final aim of this project, these surfaces were used for the nanoparticle synthesis.

Keywords: superoleophobic textured surfaces, omniphobic textured surfaces, oil droplet manipulation, photolithography, microfabrication, droplet-based microfluidic system, nanoparticle synthesis, surface texture

ÖZET

DOKULU YÜKSEK ORANDA YAĞ VE SU SEVMEZ YÜZEYLERDE YAĞ DAMLACIKLARININ KONTROLLÜ HAREKET ETTİRİLMESİ

Ecem Yelekli

Malzeme Bilimleri ve Nanoteknoloji, Yüksek Lisans

Advisor: E. Yegan Erdem Ercan

July, 2020

Mikroakışkan sistemler çoğu zaman kapalı kanallardan oluşmaktadır ve akış bu kanallarda şırınga ya da basınçlı pompa yardımı ile kontrol edilmektedir. Kanallar içerisinde olan akış damlacık halinde de olabilir. Fakat bu sistemlerde, her bir damlacığa ayrı ayrı müdahele etmek mümkün değildir. Kanal temelli yöntemlere alternatif olarak, damlacıklar yüzey üzerinde enerji gradyanı oluşturularak hareket ettirilebilirler. Bu sistemlerle damlacıklar ayrı ayrı idare edilebildiklerinden ve numuneler küçük paketler halinde taşındıklarından daha kontrollü işlemler gerçekleştirilebilmektedir. Örneğin numunelerin konsantrasyonları ve hacimleri daha hassas bir şekilde ayarlanabilmektedir. Bu sistemler özellikle biyolojik analiz ve kimyasal sentez için kullanışlıdır. Bu zamana kadar, su damlacığının yüzey enerji gradyanı kullanılarak hareket ettirilmesi literatürde gösterilmiştir. Diğer bir yandan, yağ damlacıklarının yüzey üzerinde kontrollü olarak taşınması, yağ bazlı solüsyonların düşük yüzey geriliminden dolayı hala başarılamayan zorlu bir iş olarak kalmıştır. Ayrıca, literatürde yağ damlacıklarının taşınması ile ilgili yer alan birçok çalışma sulu ortamda gerçekleştirilmiştir; fakat bu metot potansiyel kullanım alanlarını kısıtlayıcıdır.

Bu çalışmada mikrolitre ölçekli yağ damlacıklarının yüksek oranda yağ ve su sevmez (süperomnifobik) dokulu yüzeylerden yararlanılarak taşınması başarmayı

amaçlamaktadır. Yüzeye dikey olarak titreşim uygulanarak, yağ damlacıklarının histerezisin üstesinden gelmesi ve dokulu yolu takip ederek yüzey üzerinde ilerlemesi sağlanmıştır. Yağ sevmez özellik yağın yüzeye tutunmasını azaltmak için gereklidir. Bu sistem, tek bir girdi (dikey titreşim) kullanarak damlacık hareketini ayrı ayrı kontrol etme, damlacıkları hassas oranlarda karıştırma ve böylece kanallı sistemlerde karşılaşılan tıkanma ve kontaminasyon gibi problemleri ortadan kaldırma gibi avantajlara sahiptir.

Bu çalışmanın başlangıç aşaması ağırlıklı olarak topografik etkilerin yağ sevmez özelliğine olan etkisinin araştırılmasına ve yüksek oranda yağ ve su sevmez (superomniphobic) yüzey üretmeye odaklanmıştır. Yüzeyler geleneksel fotolitografi tekniği kullanılarak silikon plakalar üzerinde üretilmiştir. Bu aşamada yüzeylerde mantar mikroyapısı ve dikey kenarlı mikroyapı olmak üzere iki farklı profili kullanılmıştır. Yağsevmez özelliği elde edebilmek için, mantar mikroyapısının gerekli olduğu gözlenmiştir. Ayrıca, mikroyapıların kenar uzunluğunun, mikroyapıların arasındaki mesafenin ve TiO_2 kaplamasının ıslanılabilirlik özelliğine olan etkisi araştırılmıştır. Yağ damlacıklarının taşınması için, yüksek oranda su ve yağ sevmez özellikte dokulu yüzeyler geliştirilmiş ve bu yüzeyler titreşim uygulanarak test edilmiştir. Çalışmanın son aşamasında bu yüzeyler nanoparçacık sentezi için kullanılmıştır.

Anahtar sözcükler: yağ sevmez dokulu yüzeyler, omnifobik dokulu yüzeyler, yağ damlacıklarının kontrollü olarak hareket ettirilmesi, fotolitografi, mikro-üretim, damlacık temelli mikro-akışkan sistem, nanoparçacık sentezi, yüzey dokusu

Acknowledgements

I wish to express my sincere appreciation and deep gratitude to my supervisor, Professor Yegan Erdem Ercan, for her valuable and constructive suggestions, guidance, and continuous support she has provided during my research and study. Without her persistent help, the purpose of the project would not be realized. Further, I would like to thank the committee members of this thesis, to Professor Bilge Baytekin and Professor Ender Yıldırım for their time.

I want to thank to all members of Micro and Nano Integrated Fluids (MiNI) Research Group, Berkay Şahinoğlu, Büşra Sarıarslan, Eliza Sopubekova, Gökçe Özkazanç, Mayssam Naji, Malik Abdul Wahab, Muhammad Saqib, for their help and support.

I am thankful to the faculty and staff of UNAM and Mechanical Engineering Department for creating and maintaining a vibrant environment. Especially I thank the technicians Esra Arman Karaarslan, Fikret Piri, Dr.Gökçe Çelik, İsa Murat Çalık, Murat Güre and Semih Bozkurt for their help.

I thank all of my friends who always there for me. Especially I thank Roujin Ghaffari, Ulviyya Quliyeva, Yasamin Sheidaei for adding color to my life in Bilkent.

I owe thanks to a very special person, Çağatay Kirici, who is my closest friend and my spouse, for his love, his understanding, and most importantly for his patience. I deeply appreciate his belief in me.

Special thanks go to my beloved family. To my mother Sevgi Yelekli and my father Cezmi Yelekli for their support and encouragement during my studies and to my lovely sister Gizem Yelekli, who was always there for me as a friend and extremely supportive of me. I could not have done it without them.

Contents

List of figures

List of Tables

Chapter 1

INTRODUCTION

In the last decade, there has been a great interest in superomniphobic surfaces. Superomniphobicity refers to the super-repellency both for the high and low surface tension fluids, including water, oil, and organic liquids. Since most of the liquids contain oil and organic liquids and they wet the superhydrophobic surfaces, there is a high demand for the surfaces that repel both water and oil. Thus, there is a growing interest in the fabrication of superomniphobic surfaces exhibiting a great potential for a wide range of applications.

It is well known that a suitable combination of surface roughness and the low surface energy is essential for the fabrication of superhydrophobic surfaces and this principle applies also to the fabrication of superomniphobic surfaces. However, since oil has lower surface tension, omniphobic or oleophobic surfaces require to be much lower surface energy and it is technically challenging. To fabricate a superomniphobic surface, many studies used fluoropolymer coating that include CF_3 and CF_2 group, which have low surface energy. However, low surface tension coating is not sufficient to make a surface omniphobic. In 2007, Tuteja et al. used re-entrant microstructures in addition to the low surface energy to fabricate a superoleophobic surface[1]. This was a significant contribution to the development of superoleophobic and superomniphobic surfaces. Thus far, omniphobic surfaces are fabricated in suitable surface roughness (micro-nano hierarchical structures, re-entrant structure, micropillars, etc.) with fluoropolymer coatings.

Based on the development in the non-wetting surfaces, droplet manipulation on these surfaces has been studied by a number of researchers[2–5]. Many methods were developed to manipulate water droplets by utilizing surface energy gradients[6–20]. Although water droplet manipulation has been widely studied, oil droplet manipulation is not studied in depth and remained limited in the literature. However, since many chemical and biological samples have lower surface tension than water and most contaminants and pollutants are organic, oil droplet manipulation plays an important role especially in microfluidics, lab-on-a-chip devices, and analytical devices. Yet, creating oleophobic surfaces and moving oil droplets on these surfaces is challenging due to the low surface tension of oil and organic liquids. In the literature, oil droplet transportation was achieved mostly in aqueous phase[16,21–25] rather than ambient air[26] which restricts its usage area.

The primary objective of this research is to transport microliter-sized oil droplets in a controlled manner on superomniphobic textured surfaces and to achieve oil-based nanoparticle synthesis on these surfaces. To achieve this goal, this project divided into three main experimental parts;

1. Fabrication and characterization of the superomniphobic textured surfaces without energy gradients by a conventional microfabrication method and identifying the effect of control parameters (width of microstructures, the distance between them , their cross sectional profile) on superoleophobicity

2. Oil droplet transportation on superomniphobic textured surfaces (ratchet tracks), which is fabricated based on the optimum design based on the experimental study of surfaces without energy gradients

3. Oil-based gold nanoparticle synthesis inside droplets on the superomniphobic textured surfaces (ratchet tracks) .

In the first part, the effect of the surface texture on wettability was studied with water, hexadecane, and edible olive oil. Therefore, initially textured surfaces without energy gradients were designed to understand to obtain the desired

topography. These surfaces were fabricated by using conventional clean room methods and they were composed of pillar arrays that have two different cross sectional profiles; mushroom (re-entrant) and straight. Textured design and geometry effects on wettability were characterized by contact angle measurement system. A systematic investigation reveals that the mushroom structure is the key parameter to obtain superoleophobicity.

In the second part, the oil-droplet transportation was demonstrated. Previously, ratchet tracks were used for water droplet transportation; however, this is the first study that focuses on using them for oil droplet transportation. Design parameters for the ratchet tracks were determined based on the results obtained with surfaces without energy gradients (static surfaces). Hexadecane transportation on the fabricated ratchet tracks was achieved and the dynamics of the oil droplet movement were analyzed.

In the third part, gold nanoparticle synthesis on textured ratchets tracks was studied. Ratchet track designs were reconstructed to achieve merging of droplets for mixing reagents. Gold nanoparticle synthesis on the reconstructed ratchet tracks studied by using the edible coconut oil.

In this chapter, wetting phenomena is explained in detail and a brief literature review on superomniphobic surfaces for oil droplet manipulation is provided.

1.1. Wetting Phenomena in Nature

Wetting is related to the spread of liquid on a solid or liquid surface; and it concerns a wide range of natural systems as well as numerous industrial applications[27]. Some of these applications are related to painting in the chemical industry, treatment of automobile tires for enhancement of adhesion to icy roads, production of anti-frost glasses, and waterproof concrete for construction[28].

On the other hand, many creatures in nature use their wetting characteristics for survival. For example, Namib Desert beetle captures water from fog via its special wettable back surface consisting of hydrophobic and hydrophilic parts[29], spiders

collect water with their hydrophilic silk fibers[30] and shorebirds feed themselves by transporting prey inside droplets from the top of their beak to their mouth in a stepwise ratcheting fashion[17]. In addition to these examples, the movement of the insects on the surface of water and the transportation of water from the roots to the leaves of plants are also related to the wetting phenomena.

Surfaces on which water makes high contact angle with low contact angle hysteresis are called superhydrophobic surfaces. A very well-known example for these surfaces is the lotus leaf. Drops on the lotus leaf preserve its spherical shape by making a contact angle between 150^o and 180^o. Since it has very low contact angle hysteresis, drops move easily by slightly tilting the leaves and almost does not wet the surface. In addition, while the drops are moving, they roll rather than slide while preserving their spherical shape. Moving drops remove dust and dirt from the lotus leaf that is called as self-cleaning, a feature associated with the Lotus leaf. Due to this feature, the Lotus leaf is a symbol that represents the purity in the buddhism[31]. In addition, in favor of low contact angle hysteresis and large static contact angle, many creatures in nature carry out the task of self-transporting of the liquid droplet to maintain their lives.

Some of the superhydrophobic surfaces can have high contact angle hysteresis such as leaves of scallion and garlic[32]. Although water droplets make contact angle larger than 150^o on these leaves, when the leaves are tilted vertically, droplets stay on them. This feature provides moisture for the plants. When the surface makes low contact angle with water they are called superhydrophilic surfaces. Some plant leaves are superhydrophilic for photosynthesis. Termits *(Schedorhinotermes)* use the hydrophilic parts on their body and wings to attach the places with a large quantity of water that helps its colonization[33]. In addition, wetting phenomena is important at the micro-nano scale and it is governed by the surface tension[28].

These wetting properties were sought after for various potential applications such as in self-cleaning, anti-fogging, droplet manipulation, oil-water separation, anti-fouling, printing techniques, optical devices as wells as the lab on a chip

applications and microfluidic devices. Because of excellent non-wetting properties of superomniphobic surfaces, there is a great interest in their applications such as in self cleaning[34–36], oil droplet manipulation[37], chemical shielding[38]. One way to have these properties for our applications is to mimic the nature[39]. The physics behind the wetting phenomena is explained in the next section.

1.1.1. Theoretical Background

From the theoretical point of view, wetting is a thermodynamic process and depends on the surface energy balance at the interfaces[40]. A liquid droplet and the solid substrate initially have interface with the gas phase (air). When a liquid makes contact with the solid surface, the air-solid interface is replaced by the area of the liquid-solid interface and a new liquid-air interface is formed[41]. Finally, three different interfacial surfaces: liquid-solid, solid-air, liquid-air are formed as in Figure 1.1.

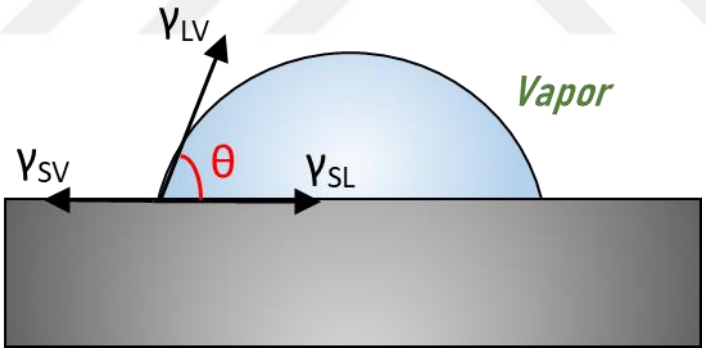

Figure 1. 1. Liquid droplet in contact with the solid substrate. At the interface of solid, liquid and gas phases, a contact angle (θ) is formed as a result of the thermodynamic balance of interfacial forces.

Each interfacial surface has its own surface energy and when a new surface forms, the total energy of the system is either decreased or increased. This energy change determines the wetting behavior of the system. Wetting is characterized by the static contact angle formed at the interface and the contact angle hysteresis, which is the difference between the advancing and the receding angles.

The static contact angle is the angle between the tangent to the liquid-gas and tangent to the solid interfaces at the contact line between the three phases and it has a value between 0° and 180° according to their wetting scale[27,42]. For instance, 0° contact angle shows complete wetting or superwetting, 180° contact angle shows complete dewetting[31]. Wetting states can be classified typically into four groups based on the static contact angle: (a) hydrophilic state, where the water droplet makes contact angle larger than 10° and smaller than 90° (Figure 1.1.2.a); (b) hydrophobic state, where the water droplet makes contact angle larger than 90° and less than 150° (Figure 1.1.2.b); (c) superhydrophilic state, where the water droplet wets the solid surface and makes a contact angle smaller than 10° (Figure 1.1.2.c); (d) superhydrophobic state, where the water droplet makes a larger contact angle than 150° (Figure 1.1.2.d)[43].

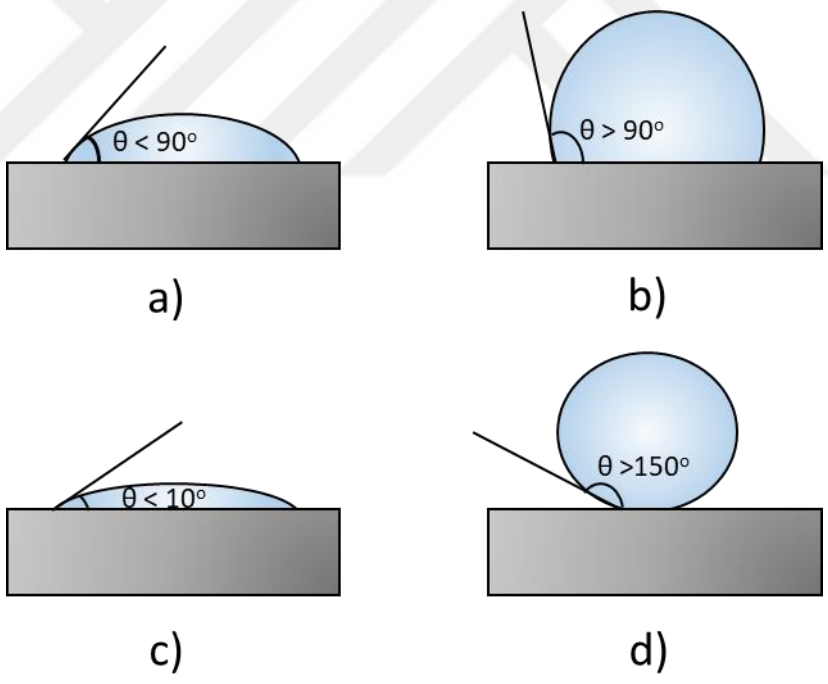

Figure 1. 2. Typical wetting states of water droplet on the solid surface a) hydrophilic state (10° < θ < 90°), b) hydrophobic state (90° < θ < 150°), c) superhydrophilic state (θ < 10°), d) superhydrophobic state (θ > 150 °).

Another important factor for characterizing the wettability is contact angle hysteresis[44]. The maximum contact angle the droplet can make on the solid

surface is termed as advancing angle (θ_{adv}) and the minimum contact angle the droplet can make is termed as the receding angle (θ_{rec}). The difference between the advancing and receding contact angles is defined as the contact angle hysteresis ($\theta_{adv} - \theta_{rec}$)[27,31,42,44,45]. The main reason for the difference between the advancing and receding is the pinning forces. These pinning forces can be due to the roughness, physical or chemical heterogeneities, and defects[31,42,44].

Contact angle hysteresis becomes prominent particularly when the droplet is in the movement. If the contact angle hysteresis is large, more energy is required to put the droplet into motion whereas, if it is small enough, the droplet is mobile and can roll even with the small forces such as blowing the air or tilting the solid surface slightly. The ability to induce droplets to roll on the surface is observed on several living beings in nature[17,29,30,39], and has inspired numerous researchers to prepare biomimetric surfaces with this property. The reason for this feature is indicated as multiscale roughness[33,46–48] that will be explained in the next section.

1.2. Effect of Surface Texture on Wetting

Wettability can be controlled by two key factors: the surface energy (chemical factor) of the surface and the roughness (physical factor) of the surface. Surface energy can be changed by introducing chemical coatings to the surface and roughness can be obtained by physically modifying the surface. The combination of these two parameters determines the wettability of the surface.

Surface roughness has a notable effect on the contact angle and contact angle hysteresis. It is important to note that, maximum contact angle on a perfectly smooth surface is about 130^{o} [39,49,50]. Thus, texturing the surface is required to have a larger contact angle and lower contact angle hysteresis. Two distinct models were developed to explain the effect of surface roughness on wettability that is called as Wenzel Model and Cassie-Baxter Model. Here, these models are explained by firstly introducing the Young-Dupré Equation.

1.2.1. Young–Dupré Equation

The Young-Dupré equation was derived around 200 years ago[51], yet it is still a fundamental concept to understand the wetting behavior. It relates the equilibrium contact angle θ_{Eq} of a droplet on the smooth surface to the surface tensions of solid-liquid (γ_{SL}), liquid-gas(γ_{LG}) and solid-gas (γ_{SG}) interfaces:

$$\gamma_{SL} + \gamma_{LG}.\cos\theta_{Eq} = \gamma_{SG} \qquad Equation\ 1.1$$

This equation is derived by the balance of the forces acting on the droplet as shown in Figure 1.1. According to Equation 1.1., if all surface tension values are known, wetting characteristics can be determined. If the surface tension of the solid-gas interface is smaller than that of the solid-liquid interface, the surface is hydrophobic. If the surface tension of the solid-gas interface is larger than that of the solid-liquid interface, the surface is hydrophilic[41]. This equation neglects the roughness, chemical heterogeneity, defects, swelling, and dissolution[28,31,52].

1.2.2. Wenzel Model

When a liquid droplet is placed on a rough surface, it can be in two different states; Wenzel and Cassie-Baxter state. It is important to note that, these models are only valid when the roughness size is very small according to the droplet size[28]. Wenzel state represents the fully wetted state and the liquid droplet is in complete contact with the rough surface as in Figure 1.3.

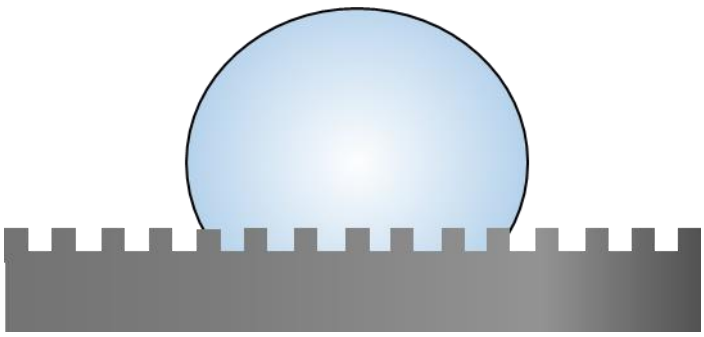

Figure 1. 3. Wenzel model

Apparent contact angle on rough and chemically homogenous surface can be calculated by the Wenzel model given as[28]:

$$\cos\theta^* = r.\cos\theta_{Eq} \qquad Equation\ 1.2$$

where the θ_{Eq} is the contact angle on the flat surface (Young-Dupré angle), r is the surface roughness and θ^* is the apparent contact angle on the rough surface. r is defined as the ratio of actual surface area to the projected surface area and it is always larger than the unity. According to Equation 1.2, when $\theta_{Eq} > 90°$ apparent contact angle becomes larger than 90^o ($\theta^* \gg 90°$) and when $\theta_{Eq} < 90°$, apparent contact angle becomes smaller than 90^o ($\theta^* \ll 90°$). Therefore, it can be stated that roughness enhances the wetting properties, by making the hydrophobic surface more hydrophobic and making the hydrophilic surface more hydrophilic[28].

Generally, liquids with low surface tension, such as oils and organic liquids have Young's angle as $\theta_{Eq} < 90°$, thus Wenzel state can not enable these liquids to have large apparent contact angles with $\theta^* < 90°$[49].

1.2.3. Cassie-Baxter Model

Cassie Baxter state represents the partially wetting state and when the liquid droplet placed on the surface, it contacts partially with the air and partially with the solid surface as shown in Figure 1.4.

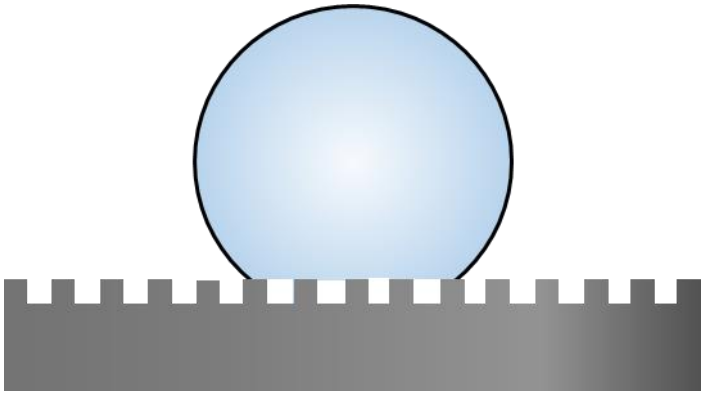

Figure 1.4. Cassie Baxter model

Apparent contact angle on rough and chemically heterogeneous surface can be calculated by the Cassie-Baxter model given as[28]:

$$\cos\theta^* = f_1 \cos\theta_1 + f_2 \cos\theta_2 \qquad Equation\ 1.3$$

where the f_1 and f_2 is the fractional areas of two different species and the θ_1 and θ_2 are the Young's contact angles on these species[28]. Fractional areas represent the unity ($f_1 + f_2 = 1$). In the case of Cassie-Baxter state, droplets are supported by the heterogeneous surface which consists of air and solid parts on which the contact angles are 180° and θ_{Eq} and fractional areas $1 - \Phi_S$ and Φ_S respectively. Thus, the equation becomes as:

$$\cos\theta^* = \Phi_S(1 + \cos\theta_{Eq}) - 1 \qquad Equation\ 1.4$$

where the θ_{Eq} is the contact angle on the flat surface (Young's angle), Φ_S is the solid fraction underneath the droplet and θ^* is the apparent contact angle on the rough surface. Φ_S is the ratio of the contact area underneath the liquid to the projected area and calculated with Equation 1.5 for the quadratic array.

$$\theta_S = \frac{b^2}{(a+b)^2} \qquad Equation\ 1.5$$

According to the Equation 1.3.4, Cassie-Baxter model results in apparent contact angles to be larger than 90° ($\theta^* \gg 90°$) not only for surfaces originally with $\theta_{Eq} > 90°$ but also for $\theta_{Eq} < 90°$. Thus, according to this model, naturally wettable surfaces can be modified as non-wettable by introducing texture. In addition, smaller solid fraction leads to having a larger apparent contact angle which means it leads to a more hydrophobic surface.

In both Wenzel and Cassie-Baxter states, droplets have different contact angles than the Young's angle. Compared to the Wenzel State, Cassie-Baxter state has lower contact angle hysteresis due to the air trapping and smaller solid fraction that the droplet contacts. In contrast to the Wenzel state, Cassie Baxter state can have a larger contact angle than 150° even for the liquids with low surface tension. Due to these features, Cassie-Baxter state is preferable in designing superhydrophobic, superoleophobic, or superomniphobic surfaces.

1.3. Superomniphobic Surfaces

Surfaces that are highly repellent to the oil and organic solvents are called superoleophobic surfaces. Most of the superoleophobic surfaces are also water repellent and have higher surface tension than oil and organic liquids. For instance, the surface tension of water is 72.3 mN/m whereas the surface tension of hexadecane is 27.5 mN/m. Superoleophobic surfaces which are repellent to water are termed as superomniphobic or superamphiphobic surfaces[53]. These surfaces have a larger contact angle than 150^{o} and contact angle hysteresis lower than 10^{o} with water, oil, and organic solvents. They have applications such as self-cleaning[54,55], anti-fouling[56], oil-water separation[57], and droplet manipulation[58]. Thus, in the last few years, there has been a growing interest in the fabrication and design of the superomniphobic surfaces and the easiest way is to fabricate such surfaces is to mimic the natural structures.

There are numerous creatures with superhydrophobic property in nature, on the other hand, creatures with superoleophobic property are rare. In particular, there are a few studies on superomniphobic bacterial biofilm colonies and pellicles, leafhoppers, and springtails[59,60,61]. Aizenberg et al. showed that bacterial biofilm colonies and pellicles have non-wetting property even for low surface tension liquids (80% ethanol, organic solvents, and biocides)[59]. Gorb et al. reported the non-wetting property of leafhoppers for high tension liquid (water), and liquids with low surface tension (ethylene glycol and diodomethane). Their integuments coated with spherical particles in 200-700 nm diameters, called as bronchosomes and the reason for the superomniphobicty is shown as the re-entrant shapes of these bronchosomes[60]. Springtail is an insect living in a soil environment and often in heavily polluted water. Werner et al. reported that springtail survives in these harsh environments with the help of the superomniphobic property on their cuticles. Their cuticles are consist of hexagonal and rhombic comb-like structures with overhang structures and endow springtails non-wetting property[61]. Consequently, inspired by the natural superomniphobic surfaces, the combination of chemical composition and multi-scale roughness is a critical parameter in designing artificial superomniphobic surfaces.

Fabrication of a superomniphobic surface is challenging due to the low surface tension of oil and organic liquids. The first artificial superomniphobic surface was developed by Tuteja et.al by introducing re-entrant structures as a third parameter to the combination of chemical composition and roughness[1]. In recent years, all the superomniphobic surfaces are fabricated based on this finding and all the fabrication methods include two processes; generation of micro-nano roughness and the functionalization with low surface energy materials. Thus, fabrication strategies can be classified into the following three types[62].

(1) The pre-roughening + post-fluorinating technique
(2) The post-fluorinating + pre-roughening technique
(3) One pot in situ fabrication technique

In the first technique, the surface was roughened firstly and then chemically modified with low surface tension materials, which is mostly fluorinated compounds. In order to create roughness, different methods can be used such as dip coating[63], photolithography[37,64], etching[65], thermal reaction[66], chemical vapor deposition[67], or electrospinning[68]. Later, the fluorinated layer can be deposited on the surface by spin-coating a fluorinated polymer solution, vapor, or liquid phase deposition.

In the second technique, fluorinated polymers or nanoparticles were synthesized firstly and then applied to flat surfaces with the help of various methods such as spray coating[69] and electrospinning[1] in order to generate roughness on the surface. In the third technique, superomniphobic surfaces can be created by one step. Li et al. prepared super- amphiphobic coatings by one-step vapor-phase polymerization treatment on fabric[70].

In this work, lithography and dry etching techniques are used to create superomniphobic surfaces. Lithography allows the structure to be precisely controlled and to be in various sizes and shapes. In addition, another advantage of the lithography process is that the mask which is using for transferring the pattern to the surface is easy to manufacture and can be used many times, resulting in

lower cost. Moreover, dry etching can be easily controlled and no residue left after the treatment[62].

1.4. Oil Droplet Transportation on Superomniphobic Surfaces

Directional droplet transportation on solid surfaces has gained interest in literature[71–73] owing to its various applications in microfluidic systems for water harvesting[11,45,74], anti-fogging[75–77], oil-water separations[16] and biomedical applications such as cell adhesion, DNA hybridization, DNA barcoding, and protein adsorption[6,78]. In nature, many creatures self-transport liquid droplets as mentioned earlier. Many of them use anisotropic wetting surfaces where the driving force is obtained by surface energy gradients. These surfaces usually have hierarchical (in micro/nano size) structures arranged in particularly one-way to achieve droplet motion[79]. Inspired by nature, in the last thirty years, some strategies were developed to conduct a directional liquid droplet motion on a solid surface by using wettability gradient[6,7,13,15,168,9,11,12,20] and these studies relied on water droplet transportation and none of these studies were focused on oil droplets.

In the literature, there are various other methods to manipulate water droplets based on the surface energy gradients achieved by electrical[80], chemical[15,81], thermal[82], and geometrical patterning (surface textured energy gradients) principles[2]. However, these methods might induce some problems for oil droplet manipulation. For instance, oil droplets cannot be manipulated by electrowetting as they are non-polar. On the other hand, a method based on thermal gradients might restrict the other processes that can be performed on the surface. During a synthesis reaction or biological process, temperature change might induce side effects and it limits its usage in biological and chemical applications. Oil droplets on the surfaces with chemical gradient do not show the high contact angle difference between the front and back edge of the droplet so that its driving force is not sufficient[83]. Because of these challenges, only a few works in the literature demonstrate oil droplet transportation by using surface energy gradients. In addition, most of the work in the literature is about controlling and transporting

oil droplets in aqueous phase[16,25], and controlling oil and other liquids with low surface tension in the ambient air have remained as a challenge.

In the literature, some studies related to oil droplet transportation aimed at directional oil droplet spreading and the principle of the spread of the drops were used in these studies[84–90]. This causes some amount of oil to remain on the surface while it is being transported and reduces its usage area. For instance, this method cannot be used in the microfluidic system, which considers the droplets as a separate individual package when manipulating the droplets. Since the droplets spread during transportation, any control over their concentration and their volume cannot be provided and that restricts its usage for the chemical reactions. As an example of these studies, Liu et al. used the capillary force in order to transport ethanol (22.10 mN/m) droplet directionally in the ambient air on the superomniphobic triply re-entrant surface[89]. This system has no external energy input and it can function on the open surface. Although it has these advantages, the transportation of liquids in the short distance (~ 3 mm). In addition to that, since the droplet was spreading on the solid surface it did not preserve its spherical shape and there was a loss of volume during transportation. Lorenceau et al. presented silicon oil (19.7 mN/m) transportation on the conical fiber and it spreads on the fiber during the transportation.

On the other hand, studies in the oil droplet transportation without continuous loss of liquid on the solid surface in ambient air is limited. Until now Li et al. achieved the oil droplet transportation in ambient air by preventing the spherical shape of the droplet during transportation. They showed self-transportation of hexadecane droplets (ylv =27.4 mN/m) on patterned oleophobic surfaces by structural wettability gradient at ambient conditions. Radially arrayed micro stripes gave the direction to the droplet towards the center by creating a continuously reducing air-liquid fraction. Oil droplets placed on the oleophobic surface self-transported towards the center of the surface and the transportation stops when the droplets reach the part where the stripes merge so that there is no control over the transportation of oil droplets. This system did not require any external energy input; however, transportation distance was limited to the radial

length of stripes so that transport was in short-range and there was no aim for continuous motion[83]. Thus, a more systematic and theoretical analysis is required for controlled oil droplet transportation on the superomniphobic surfaces.

Here, this study introduces the controlled oil droplet transportation on the superomniphobic textured ratchet tracks via vertical vibration for longer distances. Surface textured ratchet tracks are formed by the periodic arc shapes with vertical asymmetry which was initially presented by Shastry et al. for water droplet transportation[19]. Surface textured ratchet tracks enable the longer and controlled droplet transportation by transforming the random oscillations of the droplet to the net movement of the droplet with the help of asymmetric pining force that the surface creates. These tracks transport only the droplets at Fakir State.

This phenomenon is used for the water droplet transportation[10] and the water based nanoparticle synthesis[18]. In this study, this phenomenon was used for oil droplet transportation and oil-based nanoparticle synthesis. In this aspect, this project will be the first in the literature.

1.5. Overview of the Thesis

This thesis is about oil droplet transportation and oil-based nanoparticle synthesis on superomniphobic textured ratchet tracks. Chapter 2 to Chapter 4 presents the experimental studies. Chapter 2 discusses the fabrication, design parameters and characterization of surfaces used in this study, Chapter 3 discusses the theory of ratchet tracks and demonstrates the experimental studies about oil droplet transportation on the superomniphobic textured ratchet tracks, Chapter 4 discusses the surface based microfluidic systems for nanoparticle synthesis and presents the experimental findings on nanoparticle synthesis on these ratchet tracks and Chapter 5 is the conclusion part, which summarizes this work and provides suggestions for future work .

1.6. Notes to Chapter 1

1. Tuteja A, Choi W, Mabry JM, McKinley GH, Cohen RE. Designing super-oleophobic surfaces with fluoroposs. *2007 AIChE Annu Meet*. 2007;(December):1618-1623.

2. Yang JT, Yang ZH, Chen CY, Yao DJ. Conversion of surface energy and manipulation of a single droplet across micropatterned surfaces. *Langmuir*. 2008;24(17):9889-9897. doi:10.1021/la8004695

3. Zhang S, Huang J, Chen Z, Yang S, Lai Y. Liquid mobility on superwettable surfaces for applications in energy and the environment. *J Mater Chem A*. 2019;7(1):38-63. doi:10.1039/c8ta09403a

4. Ding G, Jiao W. properties for microdroplet transportation †. 2017:17325-17334. doi:10.1039/c7ta04696k

5. Mertaniemi H, Jokinen V, Sainiemi L, et al. Superhydrophobic tracks for low-friction, guided transport of water droplets. *Adv Mater*. 2011;23(26):2911-2914. doi:10.1002/adma.201100461

6. Giri D, Li Z, Ashraf KM, Collinson MM, Higgins DA. Molecular Combing of λ-DNA using Self-Propelled Water Droplets on Wettability Gradient Surfaces. *ACS Appl Mater Interfaces*. 2016;8(36):24265-24272. doi:10.1021/acsami.6b08607

7. Santos; FD Dos, Ondarquhus T. Free-Running Droplets Fabrice. *Physcal Rev Lett*. 1995;75(16):2972.

8. Daniel S, Chaudhury MK. Induced by Vibration. 2002;(8):3404-3407. doi:10.1021/la025505c

9. Daniel S, Sircar S, Gliem J, Chaudhury MK. Ratcheting motion of liquid drops on gradient surfaces. *Langmuir*. 2004;20(10):4085-4092. doi:10.1021/la036221a

10. Duncombe TA, Erdem EY, Shastry A, Baskaran R, Böhringer KF. Controlling liquid drops with texture ratchets. *Adv Mater*. 2012;24(12):1545-1550. doi:10.1002/adma.201104446

11. Fang C, Steinbrenner JE, Wang F, et al. Patterned gradient surface for spontaneous droplet transportation and water collection : simulation and experiment. *J Micromechanics Microengineering*.:115009. doi:10.1088/0960-1317/26/11/115009

12. Shastry A, Case MJ, Bo KF. Directing Droplets Using Microstructured Surfaces †. 2006;(6):6161-6167. doi:10.1021/la0601657

13. Li J, Guo Z. Spontaneous directional transportations of water droplets on surfaces driven by gradient structures. *Nanoscale*. 2018;10(29):13814-13831. doi:10.1039/c8nr04354j

14. Chu KH, Xiao R, Wang EN. Uni-directional liquid spreading on asymmetric nanostructured surfaces. *Nat Mater*. 2010;9(5):413-417. doi:10.1038/nmat2726

15. Wong B, Holbrook RJ, Wang FFY, et al. How to Make Water Run Uphill. 1992;256(June):1539-1542.

16. Yan Y, He L, Li Y, et al. Unidirectional liquid transportation and selective permeation for oil/water separation on a gradient nanowire structured surface. *J Memb Sci*. 2019;582(March):246-253. doi:10.1016/j.memsci.2019.04.011

17. Mitter C, Tilmon KJ. Surface Tension Transport of. *Smithsonian*. 2008;320(May):931-934.

18. Online VA, Bas M, Erdem EY. Soft Matter nanoparticle synthesis †. 2018:4311-4316. doi:10.1039/c8sm00091c

19. Shastry A, Taylor D, Böhringer KF. Micro-structured surface ratchets for droplet transport. *TRANSDUCERS EUROSENSORS '07 - 4th Int Conf Solid-State Sensors, Actuators Microsystems*. 2007;(July):1353-1356. doi:10.1109/SENSOR.2007.4300393

20. Chamakos NT, Karapetsas G, Papathanasiou AG. Colloids and Surfaces A : Physicochemical and Engineering Aspects How asymmetric surfaces induce directional droplet motion. *Colloids Surfaces A Physicochem Eng Asp*. 2016;511:180-189. doi:10.1016/j.colsurfa.2016.09.078

21. Zhou S, Yu C, Li C, Dong Z, Jiang L. Programmable unidirectional liquid transport on peristome-mimetic surfaces under liquid environments. *J Mater Chem A*. 2019;7(31):18244-18248. doi:10.1039/c9ta04770k

22. Tang X, Zhu P, Tian Y, Zhou X, Kong T, Wang L. Mechano-regulated surface for manipulating liquid droplets. *Nat Commun*. 2017;8:1-10. doi:10.1038/ncomms14831

23. Yong J, Chen F, Yang Q, Huo J, Hou X. Superoleophobic surfaces. *Chem Soc Rev*. 2017;46(14):4168-4217. doi:10.1039/c6cs00751a

24. Yong J, Yang Q, Chen F, et al. Reversible Underwater Lossless Oil Droplet Transportation. *Adv Mater Interfaces*. 2015;2(2):2-7. doi:10.1002/admi.201400388

25. Tian D, He L, Zhang N, Zheng X, Dou Y, Zhang X. Electric Field and Gradient Microstructure for Cooperative Driving of Directional Motion of Underwater Oil Droplets. 2016:7986-7992. doi:10.1002/adfm.201601843

26. Li J, Qin QH, Shah A, Ras RHA, Tian X, Jokinen V. Oil droplet self-transportation on oleophobic surfaces. *Sci Adv*. 2016;2(6). doi:10.1126/sciadv.1600148

27. Huhtamäki T, Tian X, Korhonen JT, Ras RHA. Surface-wetting characterization using contact-angle measurements. *Nat Protoc*. 2018;13(7):1521-1538. doi:10.1038/s41596-018-0003-z

28. de Gennes P-G, Brochard-Wyart F, Quéré D. Capillarity and Wetting Phenomena. *Capillarity Wetting Phenom*. 2004. doi:10.1007/978-0-387-21656-0

29. Desert N, Desert TN. Water capture by a desert beetle. *Nature*. 2001;414(November):33-34.

30. Zheng Y, Bai H, Huang Z, et al. Directional water collection on wetted spider silk. *Nature*. 2010;463(7281):640-643. doi:10.1038/nature08729

31. Estrela-lopis I. Soft Matter. 2009;5(1). doi:10.1039/b811945g

32. Chang FM, Hong SJ, Sheng YJ, Tsao HK. High contact angle hysteresis of superhydrophobic surfaces: Hydrophobic defects. *Appl Phys Lett*. 2009;95(6). doi:10.1063/1.3204006

33. Watson GS, Cribb BW, Watson JA. Contrasting micro/nano architecture on termite wings: Two divergent strategies for optimising success of colonisation flights. *PLoS One*. 2011;6(9). doi:10.1371/journal.pone.0024368

34. Sun D, Böhringer KF. Self-cleaning: From bio-inspired surface modification to MEMS/microfluidics system integration. *Micromachines*. 2019;10(2). doi:10.3390/mi10020101

35. Wu D, Wu SZ, Chen QD, et al. Facile creation of hierarchical PDMS microstructures with extreme underwater superoleophobicity for anti-oil application in microfluidic channels. *Lab Chip*. 2011;11(22):3873-3879. doi:10.1039/c1lc20226j

36. Zhang E, Cheng Z, Lv T, Li L, Liu Y. The design of underwater superoleophobic Ni/NiO microstructures with tunable oil adhesion. *Nanoscale*. 2015;7(45):19293-19299. doi:10.1039/c5nr05375g

37. Li J, Qin QH, Shah A, Ras RHA, Tian X, Jokinen V. Oil droplet self-transportation on oleophobic surfaces. *Sci Adv*. 2016;2(6):1-7. doi:10.1126/sciadv.1600148

38. Pan S, Kota AK, Mabry JM, Tuteja A. Superomniphobic surfaces for effective chemical shielding. *J Am Chem Soc*. 2013;135(2):578-581. doi:10.1021/ja310517s

39. Darmanin T, Guittard F. Superhydrophobic and superoleophobic properties in nature. *Mater Today*. 2015. doi:10.1016/j.mattod.2015.01.001

40. Wenzel RN. RESISTANCE OF SOLID SURFACES TO WETTING BY WATER. *Ind Eng Chem*. 1936;28(8):988-994. doi:10.1021/ie50320a024

41. Bonn D, Eggers J, Indekeu J, Meunier J, Rolley E. Wetting and spreading. 2009;81(June):739-805. doi:10.1103/RevModPhys.81.739

42. Mittal KL. *Contact Angle, Wettability and Adhesion, Volume 5*. Vol 6.; 2008. doi:10.1201/b12144

43. Koch K, Barthlott W. Superhydrophobic and superhydrophilic plant surfaces: An inspiration for biomimetic materials. *Philos Trans R Soc A Math Phys Eng Sci*. 2009;367(1893):1487-1509. doi:10.1098/rsta.2009.0022

44. Gao L, Mccarthy TJ. The " Lotus Effect " Explained : Two Reasons Why Two Length Scales of Topography Are Important. 2006:2966-2967. doi:10.1021/la0532149

45. Ueda E, Levkin PA. Emerging applications of superhydrophilic-superhydrophobic micropatterns. *Adv Mater*. 2013;25(9):1234-1247. doi:10.1002/adma.201204120

46. Nosonovsky M, Bhushan B. Biologically inspired surfaces: Broadening the scope of roughness. *Adv Funct Mater*. 2008;18(6):843-855. doi:10.1002/adfm.200701195

47. Li XM, Reinhoudt D, Crego-Calama M. What do we need for a superhydrophobic surface? A review on the recent progress in the preparation of superhydrophobic surfaces. *Chem Soc Rev*. 2007;36(8):1350-1368. doi:10.1039/b602486f

48. Dufour R, Perry G, Harnois M, et al. From micro to nano reentrant structures: Hysteresis on superomniphobic surfaces. *Colloid Polym Sci*. 2013;291(2):409-415. doi:10.1007/s00396-012-2750-7

49. Kota AK, Kwon G, Tuteja A. The design and applications of superomniphobic surfaces. *NPG Asia Mater*. 2014;6(6):1-16. doi:10.1038/am.2014.34

50. Nishino T, Meguro M, Nakamae K, Matsushita M, Ueda Y. The lowest surface free energy based on -CF3 alignment. *Langmuir*. 1999;15(13):4321-4323. doi:10.1021/la981727s

51. Ishigaki K. An Essay on Performance-Reproduction. *J Philos Sport Phys Educ*. 1995;17(1):39-55. doi:10.9772/jpspe1979.17.39

52. Liu K, Yao X, Jiang L. Recent developments in bio-inspired special wettability. *Chem Soc Rev*. 2010;39(8):3240-3255. doi:10.1039/b917112f

53. Ellinas K, Tserepi A, Gogolides E. From Superamphiphobic to Amphiphilic Polymeric Surfaces with Ordered Hierarchical Roughness Fabricated with Colloidal Lithography and Plasma Nanotexturing. 2011:3960-3969. doi:10.1021/la104481p

54. Zhao H, Law K. Directional Self-Cleaning Superoleophobic Surface. 2012. doi:10.1021/la301894e

55. Sun T, Feng L, Gao X, Jiang L. Bioinspired surfaces with special wettability. *Acc Chem Res*. 2005;38(8):644-652. doi:10.1021/ar040224c

56. Genzer J, Efimenko K. Recent developments in superhydrophobic surfaces and their relevance to marine fouling: A review. *Biofouling*. 2006;22(5):339-360. doi:10.1080/08927010600980223

57. Xu Z, Zhao Y, Wang H, Wang X, Lin T. A Superamphiphobic Coating with an Ammonia-Triggered Transition to Superhydrophilic and Superoleophobic for Oil-Water Separation. *Angew Chemie - Int Ed*. 2015;54(15):4527-4530. doi:10.1002/anie.201411283

58. Wong WSY, Liu G, Tricoli A. Superamphiphobic Bionic Proboscis for Contamination- Free Manipulation of Nano and Core – Shell Droplets. 2017:1-8. doi:10.1002/smll.201603688

59. Epstein AK, Pokroy B, Seminara A, Aizenberg J. Bacterial biofilm shows persistent resistance to liquid wetting and gas penetration. 2011;108(3):995-1000. doi:10.1073/pnas.1011033108

60. Rakitov R, Gorb SN. Brochosomal coats turn leafhopper integument to superhydrophobic state. 2013.

61. Helbig R, Nickerl J, Neinhuis C, Werner C. Smart Skin Patterns Protect Springtails. 2011;6(9):2-7. doi:10.1371/journal.pone.0025105

62. Liu H, Wang Y, Huang J, Chen Z, Chen G. Bioinspired Surfaces with Superamphiphobic Properties : Concepts , Synthesis , and Applications. 2018;1707415:1-27. doi:10.1002/adfm.201707415

63. Wang H, Zhou H, Gestos A, Fang J, Lin T. Robust, Superamphiphobic Fabric with Multiple Self-Healing Ability against Both Physical and Chemical Damages. 2013. doi:10.1021/am4029679

64. Li T, Paliy M, Wang X, Kobe B, Lau W, Yang J. Facile One-Step Photolithographic Method for Engineering Hierarchically Nano/Microstructured Transparent Superamphiphobic Surfaces. 2015. doi:10.1021/acsami.5b01926

65. Li X, Shi T, Liu C, Zhang Q, Huang X. Multifunctional substrate of Al alloy based on general hierarchical micro / nanostructures : superamphiphobicity and enhanced corrosion resistance. *Nat Publ Gr*. 2016;(October):1-11. doi:10.1038/srep35940

66. Yu J, Wang H, Yin N, Xu X. RSC Advances. 2014:24163-24169. doi:10.1039/c4ra01350f

67. Paven M, Fuchs R, Yakabe T, et al. Mechanical Properties of Highly Porous Super Liquid-Repellent Surfaces. 2016:4914-4922. doi:10.1002/adfm.201600627

68. Ganesh VA, Dinachali SS, Nair AS, Ramakrishna S. Robust Superamphiphobic Film from Electrospun TiO 2 Nanostructures. 2013. doi:10.1021/am302790d

69. Ge D, Yang L, Wang C, Lee E, Zhang Y, Yang S. A multi-functional oil–water separator from a selectively pre-wetted superamphiphobic paper. 2015:6149-6152. doi:10.1039/c4cc09813g

70. Wang H, Xue Y, Lin T. Soft Matter. 2011:8158-8161. doi:10.1039/c1sm05621b

71. Li Y, He L, Zhang X, Zhang N, Tian D. External-Field-Induced Gradient Wetting for Controllable Liquid Transport: From Movement on the Surface to Penetration into the Surface. *Adv Mater*. 2017;29(45):1-18. doi:10.1002/adma.201703802

72. Cui Y, Li D, Bai H. Bioinspired Smart Materials for Directional Liquid Transport. *Ind Eng Chem Res*. 2017;56(17):4887-4897. doi:10.1021/acs.iecr.7b00583

73. Ju J, Zheng Y, Jiang L. Bioinspired one-dimensional materials for directional liquid transport. *Acc Chem Res*. 2014;47(8):2342-2352. doi:10.1021/ar5000693

74. Garrod RP, Harris LG, Schofield WCE, et al. Mimicking a Stenocara beetle's back for microcondensation using plasmachemical patterned superhydrophobic-superhydrophilic surfaces. *Langmuir*. 2007;23(2):689-693. doi:10.1021/la0610856

75. Cebeci FÇ, Wu Z, Zhai L, Cohen RE, Rubner MF. Nanoporosity-driven superhydrophilicity: A means to create multifunctional antifogging coatings. *Langmuir*. 2006;22(6):2856-2862. doi:10.1021/la053182p

76. Rong W, Kazuhito H, Akira F, et al. Light-induced amphiphilic surfaces. *Nature*. 1997;338:431-432.

77. Chiou NR, Lu C, Guan J, Lee LJ, Epstein AJ. Growth and alignment of polyaniline nanofibres with superhydrophobic, superhydrophilic and other properties. *Nat Nanotechnol*. 2007;2(6):354-357. doi:10.1038/nnano.2007.147

78. Lai YH, Yang JT, Shieh D Bin. A microchip fabricated with a vapor-diffusion self-assembled-monolayer method to transport droplets across superhydrophobic to hydrophilic surfaces. *Lab Chip*. 2010;10(4):499-504. doi:10.1039/b917624a

79. Kong T, Luo G, Zhao Y, Liu Z. Bioinspired Superwettability Micro/Nanoarchitectures: Fabrications and Applications. *Adv Funct Mater*. 2019;29(11):1-32. doi:10.1002/adfm.201808012

80. Pollack MG, Shenderov AD, Fair RB. Electrowetting-based actuation of

droplets for integrated microfluidics. *Lab Chip*. 2002;2(2):96-101. doi:10.1039/b110474h

81. Daniel S, Chaudhury MK, Chen JC. Fast drop movements resulting from the phase change on a gradient surface. *Science (80-)*. 2001;291(5504):633-636. doi:10.1126/science.291.5504.633

82. Darhuber AA, Valentino JP, Troian SM, Wagner S. Thermocapillary actuation of droplets on chemically patterned surfaces by programmable microheater arrays. *J Microelectromechanical Syst*. 2003;12(6):873-879. doi:10.1109/JMEMS.2003.820267

83. Li J, Qin QH, Shah A, Ras RHA, Tian X, Jokinen V. Oil droplet self-transportation on oleophobic surfaces. *Sci Adv*. 2016;2(6):e1600148. doi:10.1126/sciadv.1600148

84. Chen H, Zhang L, Zhang Y, Zhang P, Zhang D, Jiang L. Uni-directional liquid spreading control on a bio-inspired surface from the peristome of Nepenthes alata. *J Mater Chem A*. 2017;5(15):6914-6920. doi:10.1039/c7ta01609c

85. Li J, Zhou X, Li J, et al. Topological liquid diode. *Sci Adv*. 2017;3(10):19-25. doi:10.1126/sciadv.aao3530

86. Lorenceau É, Quéré D. Drops on a conical wire. *J Fluid Mech*. 2004;510(510):29-45. doi:10.1017/S0022112004009152

87. Li X, Li J, Dong G. Bioinspired Topological Surface for Directional Oil Lubrication. *ACS Appl Mater Interfaces*. 2020;12(4):5113-5119. doi:10.1021/acsami.9b20345

88. Liang L, Wang W, Chen J, et al. Continuous directionalwater delivery on the 3D-printed arrowhead microstructure array. *Materials (Basel)*. 2019;12(7):1-12. doi:10.3390/ma12071043

89. Liu X, Gu H, Wang M, Du X, Gao B, Elbaz A. 3D Printing of Bioinspired Liquid Superrepellent Structures. 2018;1800103:1-8. doi:10.1002/adma.201800103

90. Chen H, Zhang L, Zhang P, Zhang D, Han Z, Jiang L. A Novel Bioinspired Continuous Unidirectional Liquid Spreading Surface Structure from the Peristome Surface of Nepenthes alata. 2016;1601676:1-6. doi:10.1002/smll.201601676

91. Meena Kumari M, Philip D. Facile one-pot synthesis of gold and silver nanocatalysts using edible coconut oil. *Spectrochim Acta - Part A Mol Biomol Spectrosc*. 2013;111:154-160. doi:10.1016/j.saa.2013.03.076

Chapter 2

SUPEROMNIPHOBIC TEXTURED SURFACES

In the preliminary study of textured ratchets designed for oil droplet manipulation, surfaces with topography but without an energy gradient is examined. A systematic approach is taken to find out the best composition that gives the highest oil contact angle. Surfaces composed of pillar arrays with are fabricated and tested.

2.1. Design and Fabrication

Wettability of solid surfaces are controlled by two factors: chemical composition and topography. Chemical composition of a surface can be modified by introducing coatings; on the other hand, topography of a surface can also be modified.

Design of textured surfaces are important to understand the wettability of oil droplets. In this work, superomniphobic textured surfaces are obtained by constructing arrays of micro-pillars. Design parameters are cross sectional side profile (mushroom or straight) and their dimensions. Side length of a micropillar is represented by the symbol *b* and the distance between the pillars is represented by the symbol *a* as shown in Figure 2.1. In addition, Figure 2.1b and Figure 2.2c illustrate respectively the side views of the mushroom and straight-sided microstructures. Mushroom profiled structures have a wide tip and narrower stem (also called as re-entrant structure) whereas straight-sided microstructures has straight vertical sides without any overhang. For convenience, a parameter named

as '*space ratio (SR)*' is introduced, which is the ratio of the gap size between the microstructures to their side length. In order to investigate the effect of microstructure dimensions on the wettability of microstructures fabricated with different side lengths and SRs, the height of the microstructures '*h*' is kept the same for consistency. In order to understand the effect of the microstructure profile on the wettability, the side length of the wide tip of a mushroom structure is kept the same with that of a straight-sided microstructure.

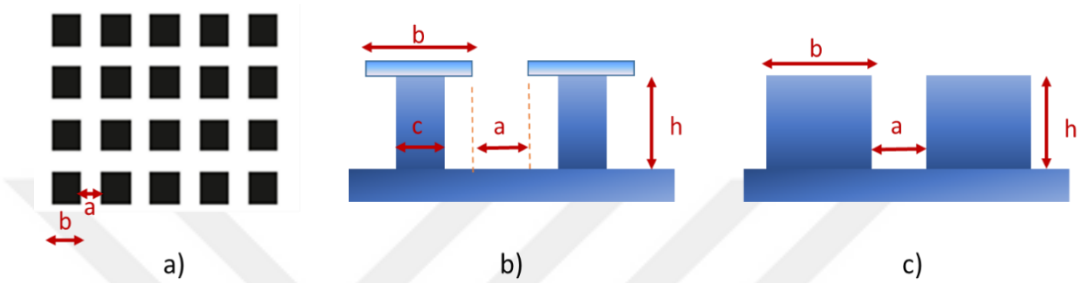

Figure 2. 1. Parameters of textured surfaces. a) Top view of the pillar array where 'b' is the side length 'a' is the gap size between the microstructures. b) Side view of mushroom microstructures. c) Side view of straight-sided microstructures.

In addition to the control parameters explained above, the effect of nano-roughness on the wettability was also investigated by introducing TiO_2 coating on top of pillar surfaces. For comparison, surfaces were fabricated in duplicate, where out of two identical surfaces, only one of them was coated with TiO_2 for comparison.

All superomniphobic textured surfaces were fabricated by using cleanroom facilities in the National Nanotechnology Research Center (UNAM).

2.1.1. Mask Design and Fabrication

Chrome photo masks used during photolithography were designed by mask layout editor software program named as ''L-Edit''. The top view of one of the mask designs is shown in Figure 2.2. The microstructure dimensions of each textured surface are listed in Table 2.1. In this work, textured surfaces with four different side lengths were used: 30 µm, 50 µm, 65 µm and 90 µm and four different SRs:

1.2, 1.6, 2 and 2.4. Thus, in terms of dimensions designed sixteen types of surfaces were designed. However, the mask includes two of them each in order to examine the TiO_2 coating effect after one fabrication. Thus, one fabricated surface was coated with TiO_2 and the other was not. These 5 inch masks were fabricated in UNAM cleanroom.

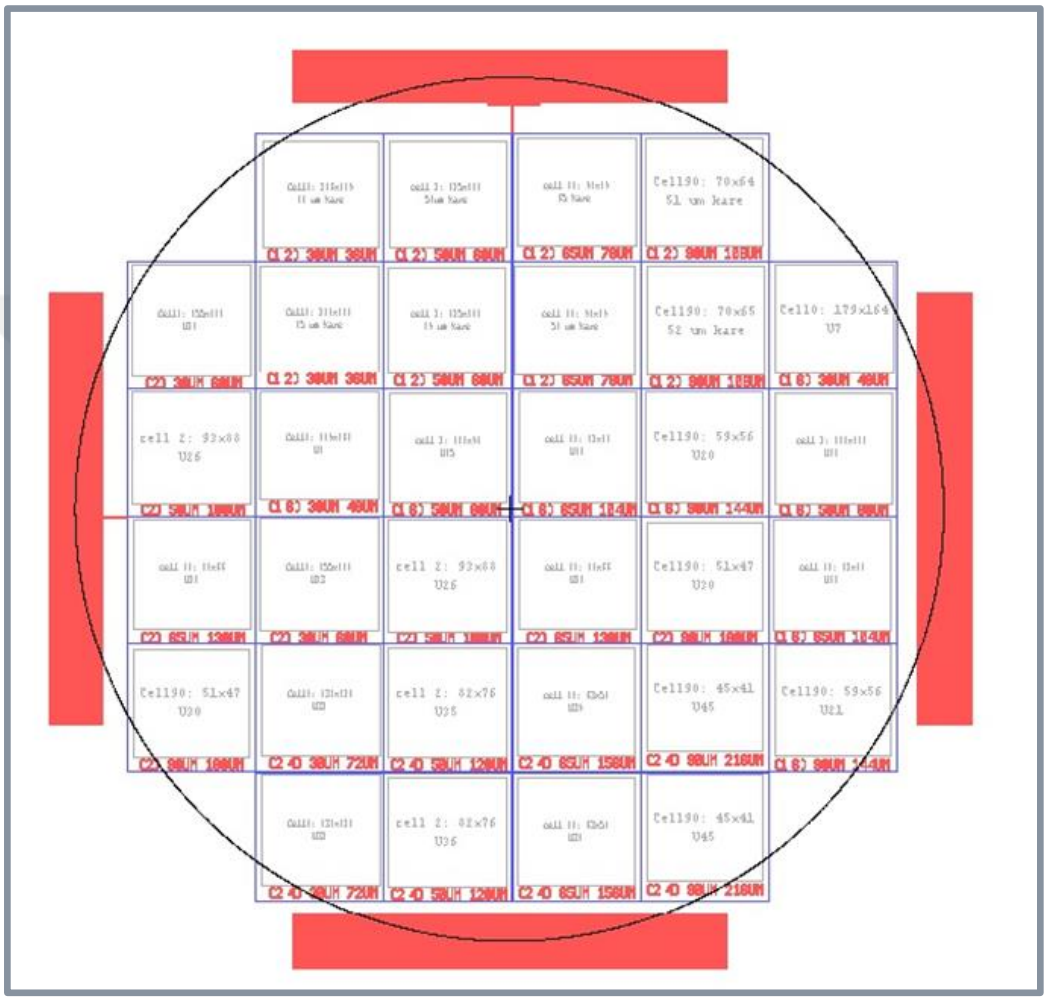

Figure 2. 2. The photomask of textured surfaces used in lithography.

Table 2. 1. Textured surface designs with different side length and space ratio of microstructures

Design #	**Side length (µm)**	**Space Ratio (µm)**
1	30	1.2
2	30	1.6

3	30	2.0
4	30	2.4
5	50	1.2
6	50	1.6
7	50	2.0
8	50	2.4
9	65	1.2
10	65	1.6
11	65	2.0
12	65	2.4
13	90	1.2
14	90	1.6
15	90	2.0
16	90	2.4

Each textured surface was patterned over an area of 13 mm×13 mm on the photomask and each textured surface was designed by square geometry. Figure 2.2 shows a part of the microstructural arrays with same space ratios (1.2) and with various side lengths of the square microstructures (30 µm, 50 µm, 65 µm and 90 µm).

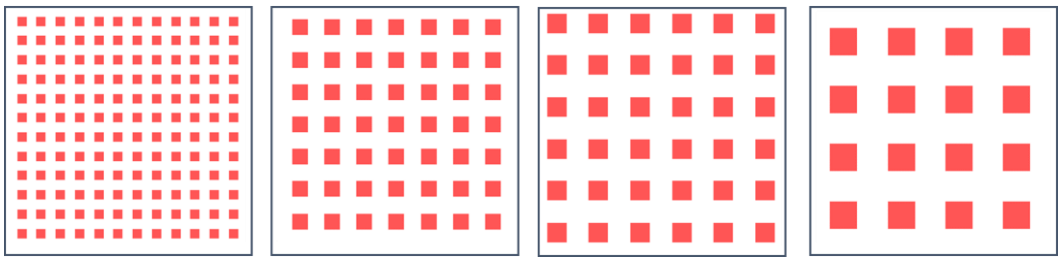

a) b) c) d)

Figure 2. 3. Textured surfaces with 1.2 SRs and with a) 30 µm side lengths b) 50 side lengths µm, c) 65 µm side lengths d) 90 µm side lengths

2.1.2. Textured Surface Fabrication

Textured surfaces were fabricated on silicon wafers (500-µm-thick p and n-type, <100>, one-sided polished) with conventional microfabrication methods that include photolithography and deep reactive ion etching. Each textured surface was fabricated with and without TiO_2 to observe the effect of nanoroughness on wettability. The fabrication process of the surfaces was shown in Figure 2.4. The silicon layer was patterned by lithography. Before each fabrication, Si wafers were cleaned by acetone, isopropyl alcohol (IPA), and distilled (DI) water, respectively. After the cleaning, wafers were dried by N_2 and baked in an oven in order to remove the moisture from the surface and enhance the photoresist adhesion.

For the superoleophobic straight sided surfaces; after cleaning, the wafer was spin coated with Hexamethyldisilazane (HMDS) for 40 seconds at 5000 rpm spin speed and 2000 rpm/s acceleration and then baked in an oven for 10 minutes at 110^oC. HMDS is a commonly used adhesion promoter and it enhances the adhesion between photoresist and silicon layer by making the surface hydrophobic. After the wafer was cooled to room temperature, it was spin coated with AZ 4533 positive photoresist for 40 seconds at 2000 rpm spin speed and 700 rpm/s acceleration. According to the datasheet, these settings provide a thin film of 4.67 µm photoresist on the wafer surface. After soft-baking at 110^oC for 2.5-3 minutes on a hot plate, the wafer was exposed to UV light in Mask Aligner with the photomask mentioned in 2.1.1. section. The recipe used in Mask Aligner determined as manual top side, transparent, constant dose, soft contact by setting the gap of 150 µm between the wafer and the mask and 250 mJ/cm^2 exposure dose. Mask thickness is 2.3 mm, the substrate thickness is 0.5 mm and photoresist thickness is 5 µm. Then, the wafer was developed in 1:5 AZ 400K solution for 2 minutes. The photoresist used in this process was positive, thus the part where the UV light exposed became soluble in the development and the other part became insoluble and the pattern was obtained. For further examination, and to make sure that the obtained pattern is the same as in the photomask, an optical

microscope was used. Then, the substrate was postbaked at 115 ^{o}C for 1 minute on a hot plate.

Before starting the etching process, the wafer was cut into smaller pieces by dicer saw so that the etching rate can be reduced since the unfunctional parts were removed. Then, the wafer was etched by a dry etching by using the Bosh process in ICP (Inductively coupled plasma). Bosh process is an anisotropic etching method for silicon etching and composed of subsequent steps; (1) etching silicon in SF_6 plasma (2) deposition of the inert polymer layer in C_4F_8 plasma to prevent from further silicon etching (3) removing inert layer on the horizontal surface with the help of the directional accelerated ions in the plasma. In our recipe, one cycle of the Bosh Process consists of 7 seconds coating and 10 seconds etching. Cycles were repeated a couple of times until the desired etch height achieved is around 10-15 µm. After the photoresist was removed by acetone, half of the surfaces were coated with 60 nm thick TiO_2 by the atomic layer deposition and the other half was not coated. Finally, all the straight sided surfaces were coated with octafluorocyclobutane (C_4F_8, similar to Teflon) gas in ICP.

A slightly different process was used to fabricate textured surfaces with mushroom microstructures. First, silicon dioxide (1µm) was deposited on a silicon wafer by plasma enhanced chemical vapor deposition (PECVD). Later, the SiO_2 layer was patterned by photolithography and etched (1µm) until the silicon surface was reached by using dry etching process in CHF_3/O_2 plasma via ICP. Then, anisotropic dry etching of silicon by the Bosh process and isotropic dry etching of silicon by Xenon difluoride (XeF_2) etching was accomplished. The XeF_2 etching consist of 5 cycles and each cycle takes 40 seconds. The pressure of nitrogen was set to 2.5 torr and the pressure of xenon difluoride was set to 10 torr. Isotropic XeF_2 etching was crucial to obtain re-entrant structures with undercut shapes (mushroom microstructures). After isotropic etching of silicone, the photoresist was removed by acetone. Half of the surfaces were coated with 60 nm with TiO_2 and the other half was not. To reduce the surface energy, C_4F_8 was coated on the surface.

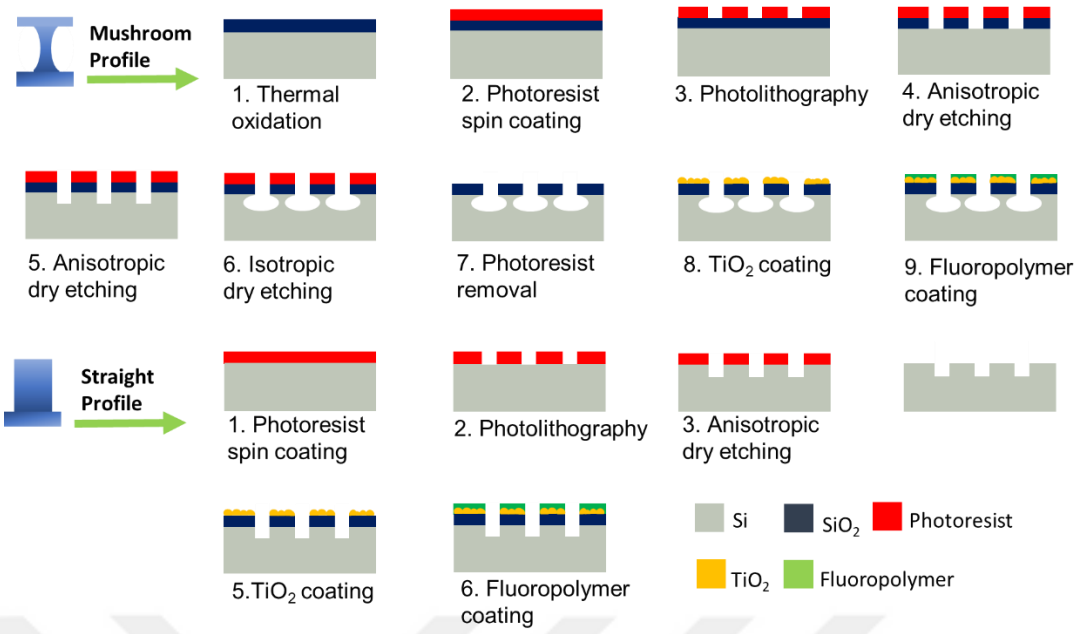

Figure 2. 4. Fabrication process of superoleophobic surfaces with a) mushroom and b) straight profiles.

2.2. Characterization

Scanning Electron Microscopy (SEM) was used to observe the topography of the fabricated textured surfaces.

Wettability of fabricated surfaces was characterized by static contact angle measurements using contact angle measurement system (Data Physics OCA30). This system is based on sessile goniometry method which is an optical method and determines the contact angle with the shape of the droplet by a fitting the shape of the droplet with the help of image processing software system. Static contact angles of distilled water (γ_w=72 mN/m), edible olive oil (γ_o=30-35 mN/m) and hexadecane (γ_H=27.47 mN/m) were measured on fabricated textured surfaces in ambient air and at room temperature. Water was dispensed on the surface in the droplet shape automatically with Hamilton Gastight 1750 syringe and SNS052/026 needle whereas olive oil and hexadecane were dispensed by the micropipette (ISOLAB) that has compatible tips for the low surface tension liquids (Brand Pipette Tips low retention). The volume of the droplets were 5 µL.

2.3. Results and Discussion

Textured surfaces fabricated by conventional lithography method and followed by the fluoro-based coating on the surfaces were observed with Scanning Electron Microscope (SEM). Figure 2.5 shows the SEM images of textured surfaces with 65 µm side size and 1.2 space ratio (65 µm (1.2)) with both mushroom microstructures as shown in the Figure 2.5a-c and straight-sided microstructures as shown in the Figure 2.5d-f.

Figure 2.5a shows the side profile of a fabricated straight microstructure. According to that SEM image, fabricated mushroom microstructures are 13.28 µm in height, 63.07 µm in side length and 76 µm in distance between the microstructures. In another words, it is nearly 1.2 space ratio (the ratio of distance between the microstructures to the side length). Also, microstructures have C_4F_8 coating with 4.72 µm thickness and this surface modification was uniform.

Figure 2.5d shows the side profile of a fabricated mushroom microstructure. According to that SEM image, fabricated straight microstructures are 12.10 µm of height, 63.51 µm of side length and 76.15 µm of distance between the microstructures with 1.2 space ratio. In addition, the cap of the microstructure was composed of SiO_2 with 1 µm thickness and has C_4F_8 coating in on top of it with 3.72 µm.

Comparing the dimensions of the fabricated microstructure with the photomask dimensions, there is nearly 2 µm shrinking in side length of the microstructures due to the development and etching processes. However, that shrinking is not significant amount so that it is negligible. Comparing the height of the mushroom and straight-sided microstructures, there is a negligible difference between them due to the etching process.

Figure 2.5b-c and Figure 2.5e-f shows the uniformity of the fabricated microstructures. Thus, it is feasible to be comparable with each other.

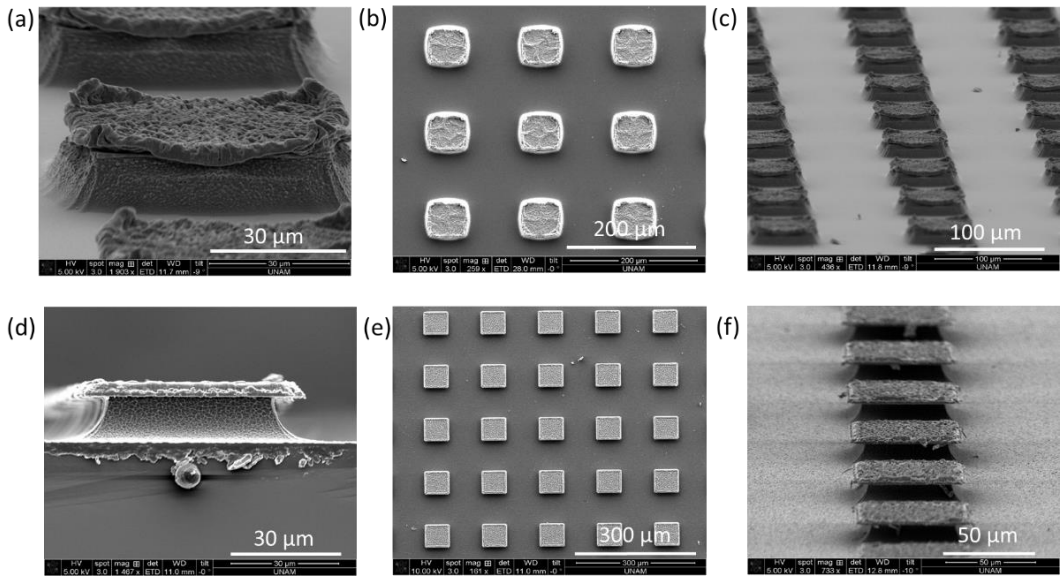

Figure 2. 5. SEM images of the fabricated microstructures in square geometry with straight profile (a,c) and mushroom profile (e,g) with side view, top view and tilted profile respectively.

Static contact angle measurement was performed with water, olive oil and hexadecane droplets on flat silicon surfaces and textured silicon surfaces without any coating in order to examine the effect of textured on the wettability. Then, contact angle measurement with the same liquids performed again on the flat and textured surfaces but this time with TiO_2 and C_4F_8 coating. Figure 2.6. shows the results of this experiment by the optical images taken by contact angle measurement system.

According to the results, the apparent contact angles (CA) for DI water, olive oil and hexadecane were 65.6 º, 30.7 º and 12 º respectively on the flat silicon surface which shows that this surface intrinsically is both oleophilic and hydrophilic so that all the droplets are in Wenzel State. On the other hand, by lowering the surface energy and adding the nanoroughness on the flat surfaces, CAs increased roughly 40 º and became 107.6 º, 68.8 º and 53 º for DI water, olive oil and hexadecane respectively. This surface modification makes the flat silicon surface hydrophobic, however it did not result in oleophobicity. Later CA measurements were performed on the silicon textured surfaces fabricated with mushroom profiled microstructures that have 50 µm side length and 1.2 space ratio.

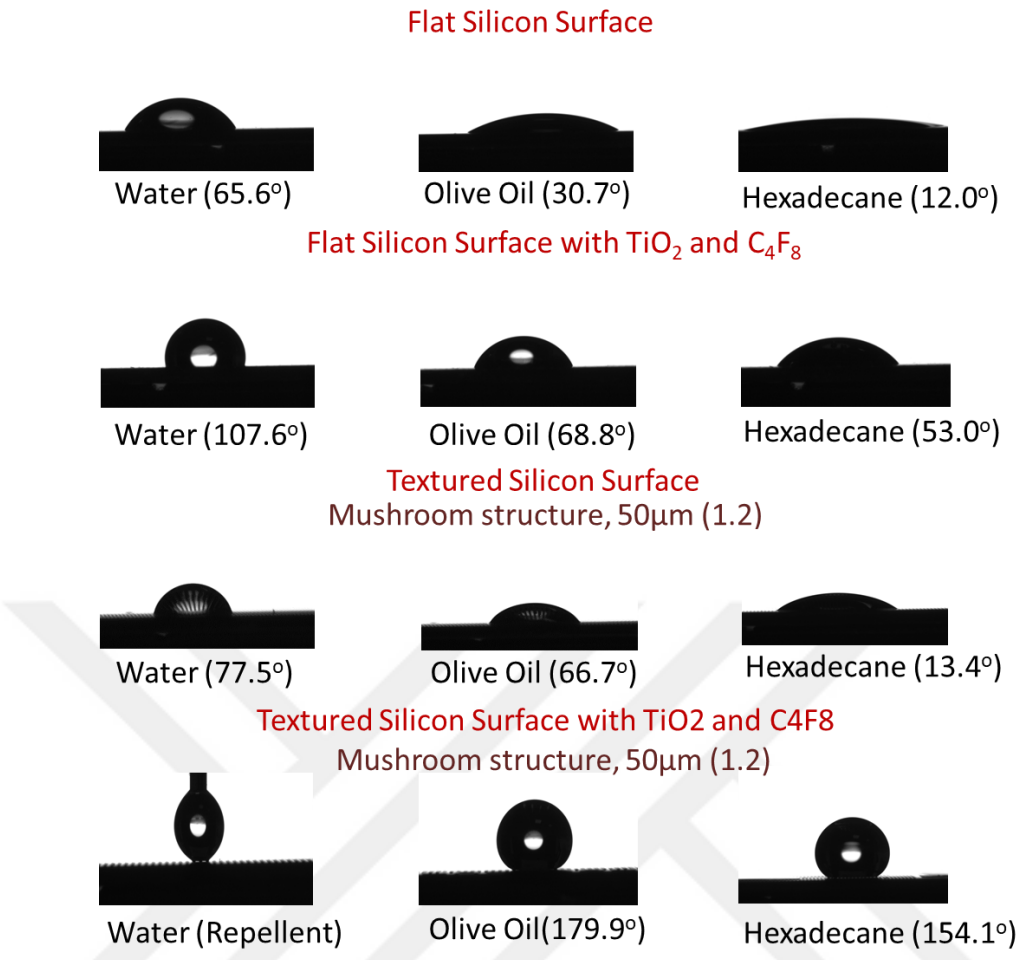

Figure 2. 6. Optical images taken by the contact angle measurement system for water, olive oil and hexadecane droplets and their contact angles on flat, coated and textured silicon surfaces.

For the first measurement on these surfaces CAs were 179.5 ° and 157.9 ° for olive oil and hexadecane whereas the DI water droplet was no able to attach to the surface due to superhydrophobicity. However with a small perturbation, moving the stage gently, CAs sharply decrease. Thus, it is concluded that surface switch from Cassie-Bexter state to Wenzel state. After cleaning the surfaces, for the second measurement, CAs were 77.5 °, 66.7 ° and 13.4 ° on the silicon textured surface for water, olive oil and hexadecane, respectively. Comparing this CA results with the CA results on the flat silicon surface, there is a significant increase however, texturing the surface was not enough by itself to make the surface oleophobic and hydrophobic. Finally, TiO_2 coating and C_4F_8 surface treatment was applied to the fabricated textured surfaces and CAs were measured as 179.9 ° for

olive oil and 154.1 ° for hexadecane and surface was reppellent to the DI water. Droplets were stable and did not collapse with a perturbation and for the other measurments, CAs were the same so that finally superomniphobic surfaces were created. Thus, it can be understood that texturing and surface treatment were concurrently required to make the surface oleophobic and hydrophobic.

Figure 2.7 shows the results of CA measurments of DI water, olive oil and hexadecane droplets on 16 different types of fabricated textured surfaces (combination of four different side lengths and four different SRs). Figure 2.7a-b shows CAs on the textured surfaces consist of straight sided microstructures, with and without TiO_2 coating and Figure 2.7c-d shows the CAs on the textured surfaces consist of mushroom microstructures with and without TiO_2 coating, respectively.

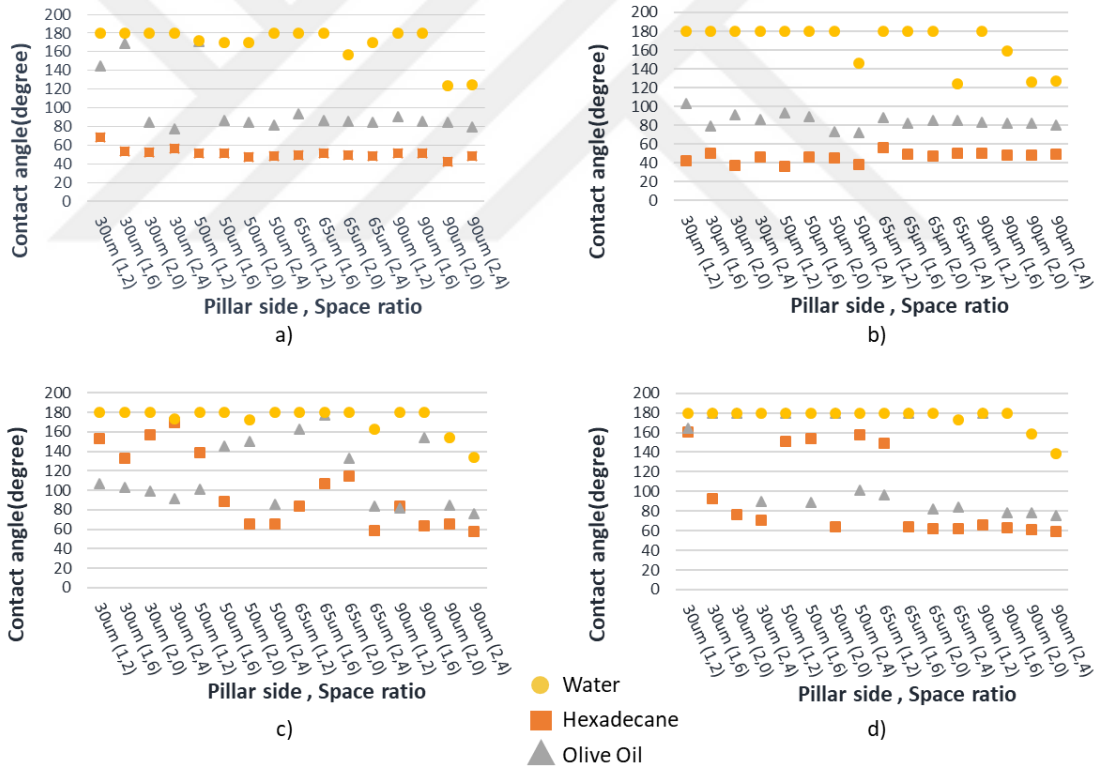

Figure 2. 7. Contact angle graphs of DI water, olive oil and hexadecane on the textured surfaces that a) consist of straight-sided microstructures and with TiO_2 coating b) consist of straight-sided microstructures and without TiO_2 coating c) consist of mushroom microstructures and with TiO_2 coating d) consist of mushroom microstructures and without TiO_2 coating

It is important to note that, results shown in the graphs are the averages of CAs taken on five different spots on the same surface. In addition, when there was no spot for testing, surfaces were cleaned by IPA and DI water respectively and dried by N_2 gas. According to the measurements, except surfaces with 90 µm side length and with 2.0 and 2.4 SRs, all the fabricated surfaces showed superhydrophobicity by making CA around 180^o with DI water droplet. Surfaces with straight-sided structures had CAs between 40 ^{o} and 60 ^{o} with hexadecane and CAs between 80^o and 100 ^{o} with olive oil. Therefore, these surfaces are repellent only to olive oil but not to hexadecane. In addition, results also showed that hexadecane droplets had approximately the same CA on surfaces with straight microstructures regardless of the space ratios and side lengths, which is same as the CA (53^o) on flat surface with TiO_2 and fluoropolymer coating as shown in the Figure 2.6. In the sharp contrast, some surfaces with mushroom microstructures made higher CA than 150 ^{o} with hexadecane and olive oil and superoleophobicty and Cassie-Baxter state was maintained. These surfaces were with side length and space ratio of 30 µm (1.2), 30 µm (2.0), 30 µm (2.4), 50 µm (1.2), 50 µm (1.6), 50 µm (2.4) and 65 µm (1.2). In addition, some of them shows repellency to the hexadecane droplets and hexadecane droplets were not able to be placed on the textured surfaces.

The experiment results also show that TiO_2 coating increased the repellency only for surfaces with side length and space ratio of 30 µm (1.2), 50 µm (1.2), 50 µm (1.6), 50 µm (2.4) and 65 µm (1.2). In addition, maximum contact angle of hexadecane achieved in this work is 164^o on the surface with 65 µm side length and 1.2 space ratio (65 µm (1.2)). According to the mean value of the contact angles, the most superomniphobic surfaces for hexadecane droplets achieved on this work are 30 µm (1.2), 30 µm (2.0), 30 µm (2.4), 50 µm (1.2), 50 µm (1.6) and 65 µm (1.2). This shows us that as the side length increases SRs can maintain the superomniphobicity decreases. Thus while mushroom structured arrays with 30 µm side length can maintain superomniphobicity with all the range of SRs except 1.6, the one with 65 µm side length can maintain superomniphobicity with only one SR which is the smallest as 1.2. This could be due to the fact that as the distance between the microstructures are getting larger, droplets penetrates into

the structures and becomes in Wenzel State causing lower CA. For example, for the microstructures with 50 µm side length, SR should be equal or lower than 1.6 to maintain the superomniphobicity on the other hand for the 65 µm side length, SR should be equal or lower than 1.2.

2.4. Conclusion

This chapter shows the fabrication of the superomniphobic textured surfaces and their characterization. A simple fabrication process for superomniphobic textured surfaces was developed to obtain microstructural arrays with a mushroom profile and C_4F_8 surface treatment. It was concluded that both introducing surface texture and low surface energy coating are crucial for the superomniphobicity. Mushroom profiled microstructures have been used by many research groups for creating superoleophobic or superomniphobic surfaces. Our research study not only examined the profiles on wettability, it also examined the effects of space ratio, side length and TiO_2 coating on wettability. In that content, several notable findings were derived from the CA measurement experiment. It was concluded that surfaces with both straight and mushroom profiled pillar arrays can be superhydrophobic. On the other hand, mushroom profile is required to maintain superomniphobicity. It is concluded that some textured surfaces fabricated with mushroom profile achieved superoleophobicity and superomniphobicity. These surfaces were with side length and space ratio of 30 µm (1.2), 30 µm (2.0), 30 µm (2.4), 50 µm (1.2), 50 µm (1.6), 50 µm (2.4) and 65 µm (1.2). As the distance between the microstructures gets larger, droplets become conformal with the surface by penetrating the structures and CA becomes lower. Finally, it was observed that TiO_2 coating increased the oleophobicity of textured surfaces with side length and space ratio of 30 µm (1.2), 50 µm (1.2), 50 µm (1.6), 50 µm (2.4) and 65 µm (1.2).

Chapter 3

OMNIPHOBIC TEXTURED SURFACES FOR OIL DROPLET MANIPULATION

In the study of oil droplet manipulation, textured ratchet tracks were fabricated based on the results with static surfaces. In addition, mushroom profile was used. Oil droplets were tested on these ratchet tracks and their dynamic behavior were examined.

3.1. Theory of Transportation of Oil Droplet on Textured Ratchet Track Surfaces

Textured surfaces can be used to create surface energy gradients for droplet manipulation in Fakir State. First work on droplet transportation by using textured surfaces was demonstrated by Shastry et al.[1] In this work, they used solid-liquid area fraction as surface energy gradient and droplets moved to larger contact area in order to reduce their surface energy. This movement was achieved by overcoming the contact angle hysteresis and viscous drag (impeding forces) with the help of a vertical speaker vibration. However, droplet transportation was not in the long range. Later, Shastry et al. demonstrated another surface design for droplet transformation, which is called as textured ratchet tracks [2]. This new design consists of periodically placed arc shapes and the droplet transportation accomplished in longer ranges. Ratchet tracks were used in various studies for

water droplet transportation[3, 4]. However, all this previous work was focusing on water droplet transport and these tracks were not used for low surface tension liquids. This is the first study that uses this concept for oil droplet transportation.

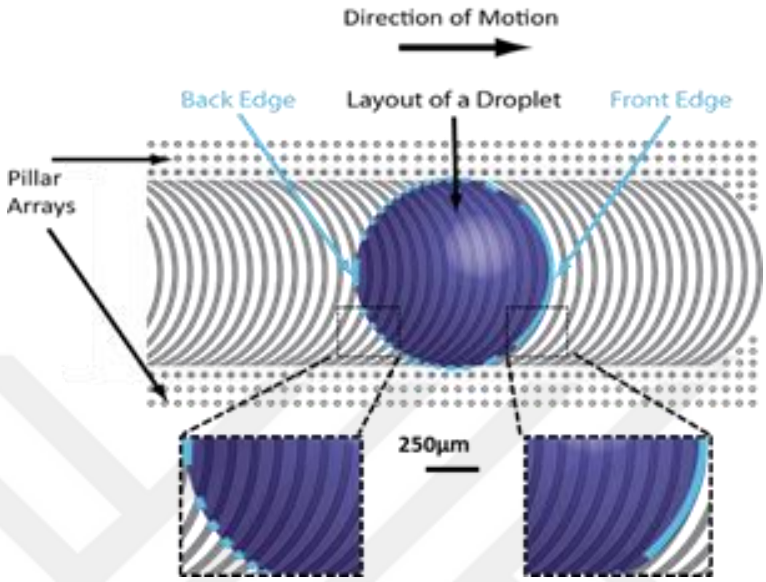

Figure 3. 1. Top view of the ratchet track used for droplet transportation with a representative droplet layout on top of it.

When a droplet is placed on the ratchet track, back and front edge of the droplet contacts differently due to the asymmetry of the ratchet track. Figure 3.1 emphasizes the asymmetry of the edges of the droplet as it is on the ratchet track. According to this figure, front edge curves in the same direction of the arc whereas back edge curves in the opposite direction. The front edge of the droplet makes a larger contact area than its back edge. Thus, droplet pins front edge more than the back edge.

When the vertical vibration is applied at the threshold value of acceleration and frequency, the contact line begins to oscillate. At that time, contact lines expand and contract with each vibration cycle. If the acceleration and frequency are below this threshold, the contact line is pinned to the surface[4]. At the driving frequency and amplitude combination, when the stage moves up, both of the edges move outward and droplet makes advancing angle (wetting), whereas when the stage moves down, both of the edges move inward and droplet makes the receding

angle (dewetting). As the droplet makes advancing and receding angles, there is always a difference between the contact angles of the front and back edges because the front edge of the droplet pins more due to the design of the track. Advancing contact angle at the front is larger than advancing contact angle at the back and receding contact angle at the front is smaller than the receding contact angle at the back. However, the difference between the advancing and receding angle (hysteresis) of the back edge larger than the one of the front so that the droplet tends to move to the front edge with each vibration cycle[3]. This results in rectifying unidirectional lateral transportation by vertical vibration.

3.2. Fabrication and Design

The same concept of the ratchet track as in Shastry et al. was used in this work[19], however; there were some differences in design parameters and fabrication steps, which will be discussed in this section.

As discussed in the Chapter 1, oil droplets can be in Fakir State only when the surface is oleophobic enough. Textured ratchet tracks were designed according to the experimental results on textured surfaces without energy gradients. It was found that the side length-space ratio combinations of 30 µm (1.2), 30 µm (2.0), 30 µm (2.4), 50 µm (1.2), 50 µm (1.6) and 65 µm (1.2) gave the best results. Therefore, these geometrical ratios were applied in creating the ratchet tracks.

These tracks were fabricated with mushroom profiles. Fabrication process was the same as the one described in Figure 2.4. It is important to note that, TiO_2 coating was used in fabrication of all ratchet tracks. The mask used for this fabrication was shown in Figure 3.2. and the list of ratchet tracks designs were shown on the mask (Table 3.1). Two different radius of curvature values (Roc) were used: 0.9 mm and 1.2 mm. All the tracks were 3 cm long. Tracks with 0.9 mm width had Roc as 1.6 mm and tracks with width 1.2 mm had Roc of 2.0 mm. Radius of curvature plays an important role for the movement of the droplet and it should be sufficient to pin the droplet's front contact line. Besides, sides of the tracks were occupied with a pillar array to provide a super repellent area to prevent droplets from falling out

of the track. Images of two ratchet tracks on the mask are showed in Figure 3.3. and Figure 3.4.

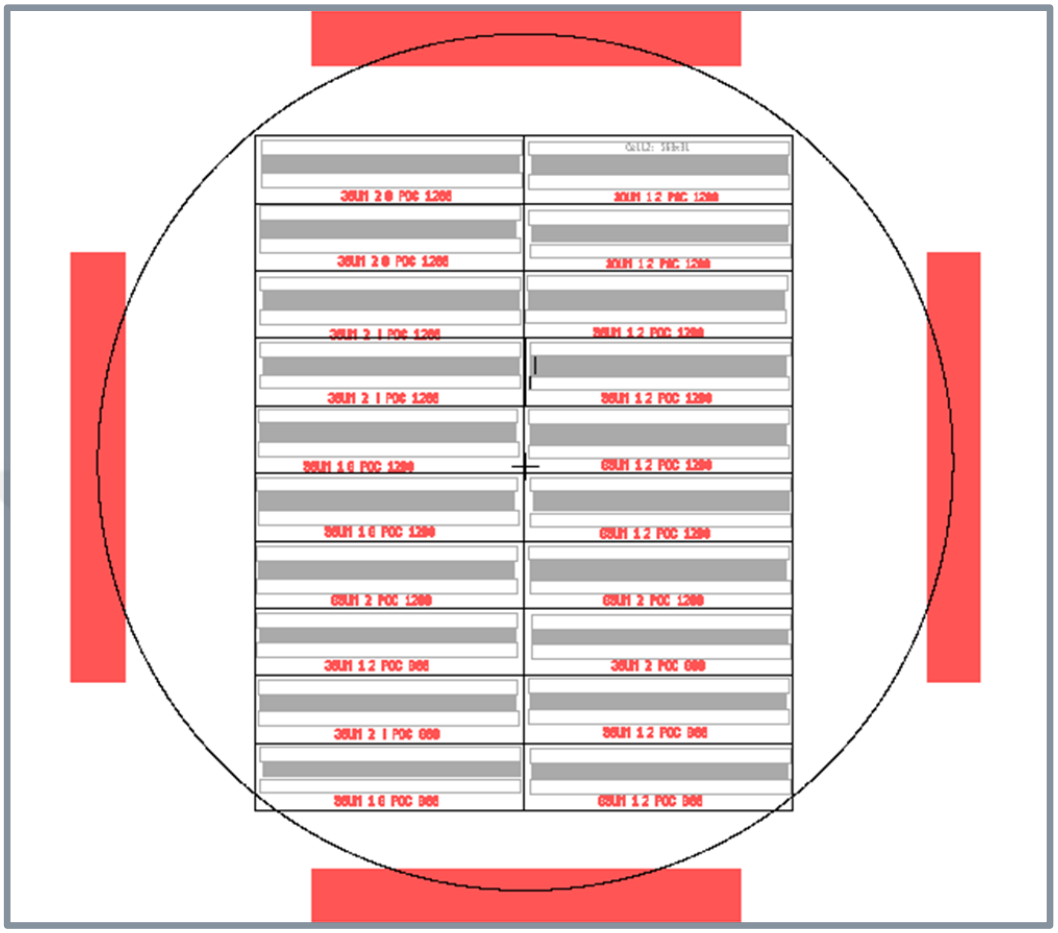

Figure 3. 2. The mask used for the fabrication of textured ratchet tracks

Table 3. 1. The table of ratchet track designs

Design number	Arc width (µm)	Space ratio	Radius of curvature (µm)
1	30	1.2	900
2	30	2.0	900
3	30	2.4	900
4	50	1.2	900
5	50	1.6	900
6	65	1.2	900
7	30	1.2	1200

8	30	2.0	1200
9	30	2.4	1200
10	50	1.2	1200
11	50	1.6	1200
12	65	1.2	1200

According to the design images shown in Figure 3.2.2 and Figure 3.2.3., although the same geometrical ratios (arc width and space ratio) were used, there is a slight difference in the width of tracks. This difference is formed due to the difference in radius of curvature.

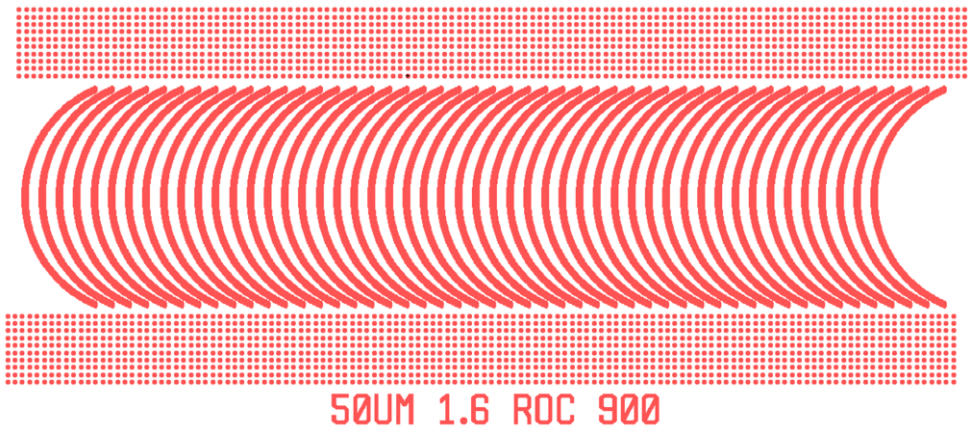

Figure 3. 3. The ratchet track design with 50 µm arc width, 1.6 space ratio and 0.9mm (900 µm) of the radius of arc curvature.

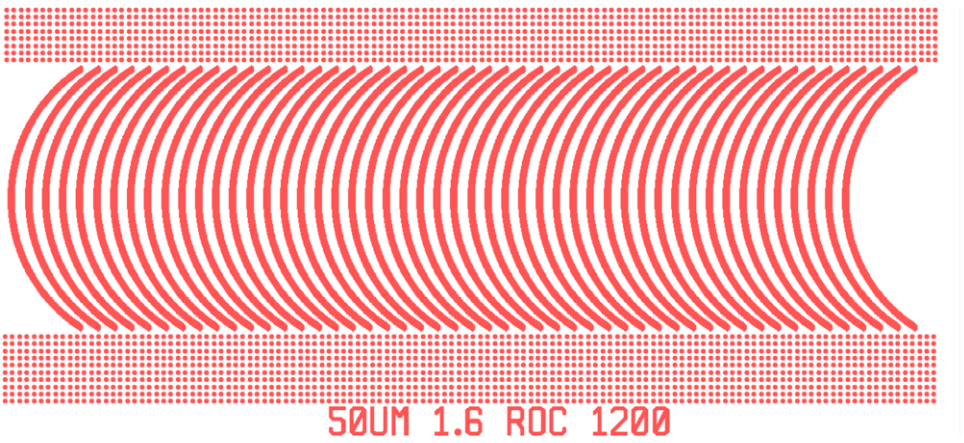

Figure 3. 4. The ratchet track design with 50 µm arc width, 1.6 space ratio and 1.2 mm (1200 µm) of the radius of arc curvature.

3.3. Experimental Methods

Fabricated ratchet tracks were tested for oil droplet transport by using the experimental set-up shown in Figure 3.5. It is composed of a function generator (GW Instek-type SFG 2004), a power amplifier (Bruel kjaer- type 2718), a vibration exciter (Brüel & Kjær Type 4809), an accelerometer, an oscilloscope (DSO-X2012A), a high speed camera (Phantom) and a high intensity light source.

The function generator produces a signal and the power amplifier enhances this signal and gives it to the vibration exciter. With the vertical vibration, droplets placed on the track can move through the direction of the front edge. It is important to note that, in order for the droplet to begin its movement, a combination of a threshold value of the amplitude of vertical vibration and excitation frequency is required. Acceleration was measured by using an accelerometer and frequency value is set through the function generator.

Hexadecane, olive oil (30-35 mN/m) and coconut oil (32.6 mN/m) were used for transportation and unless otherwise is specified, droplets were 4 µL. Droplet movement was recorded with the high speed camera and then the image data were processed by to characterize droplet motion.

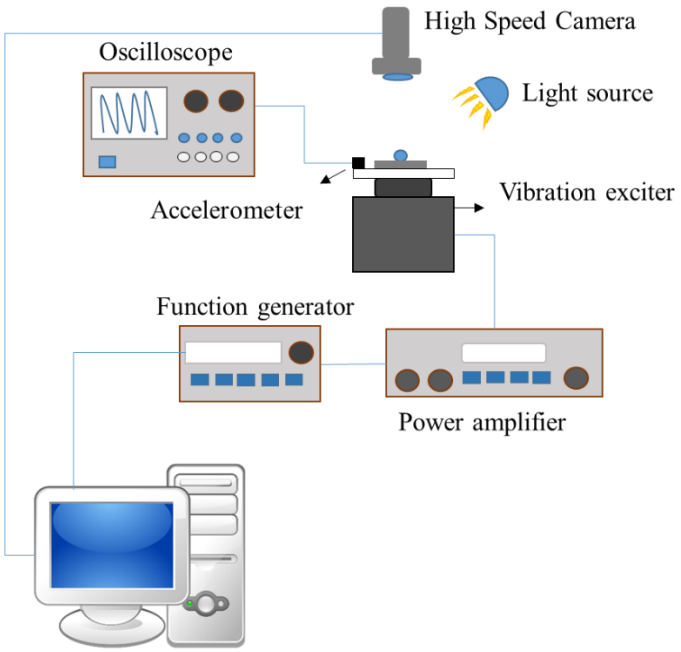

Figure 3. 5. Schematic of the experimental set-up.

3.4.Results and Discussion

Oil droplets (olive oil, coconut oil and hexadecane) were making high contact angles and they were all in Fakir State. Vertical sinusoidal vibration with 15-65 Hz frequency and 2-17 g acceleration was applied. For each set of experiment, frequency is set to a value and amplitude of acceleration was gradually increased from 0 to 15 g. The value at which droplet begins to move is recorded as the threshold value. After the experiments, only the hexadecane droplet achieved transportation on the textured tracks with 900 µm Roc. The movement was not observed on textured tracks with 1200 µm Roc.

The best three tracks on which the droplets were transported were noted as 50 µm (1.6), 50 µm (1.2) and 65 µm (1.2). All the tracks were able to transport the hexadecane droplet at a 43 Hz frequency and nearly the same acceleration value. Movements on these tracks were recorded as the video by high speed camera and as a result of image processing graphs of contact angle versus time and drop position versus time were obtained.

Figure 3.6. shows the hexadecane droplet (4 µL) movement on the ratchet track surface with 50 µm (1.6). Droplet started moving at the 43 Hz and 8.8 g. This was the minimum acceleration value for the droplet to initiate the movement at 43 Hz and can be called as ''threshold value of acceleration''. Images taken at 2 s intervals show that the shape of the droplet changes during the movement on the ratchet track. As in the theory explained in Shastry work[2], this shape change is due to the alternating wetting and dewetting behavior of the droplet and it continues to change as long as the vertical vibration applied. With the vibration, contact line oscillates and this oscillation turns into a net movement due to the asymmetry of the design. Consequently, the front and back edges of the droplet change differently during the movement. In order to analyze this change and understand the mechanism of hexadecane transportation, video is processed and graphs were obtained as in Figure 3.7.

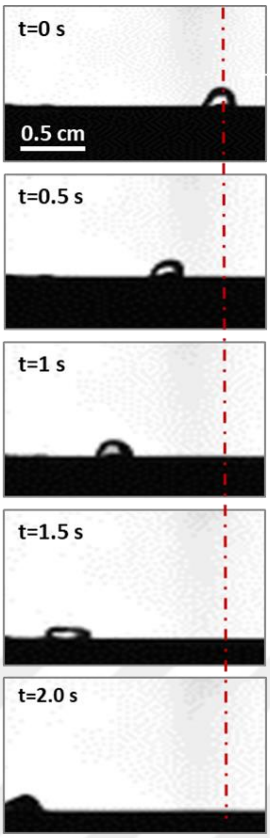

Figure 3. 6. Images of hexadecane droplet (4 µL) transported on the ratchet track of 50 µm (1.6) taken by high-speed camera. Transportation at 43 Hz and 8.8 g.

Figure 3.7. shows the graph of droplet position and contact angles of the front and back angles over time. From the droplet position versus time graph, the average velocity of the hexadecane droplet was found as 8.13 mm/s. Besides, the graph of contact angles versus time analyzes the difference in the hysteresis (the difference between the advancing and receding contact angles) of the back and front edge during the motion of the droplet. As it was explained in the previous section, front edges pin while back edge remains dynamic. Therefore, the graph shows the larger hysteresis at the front edge. The peaks show the time when the stage moves up (advancing angle) and troughs show the time when the stage moves down (receding angle).

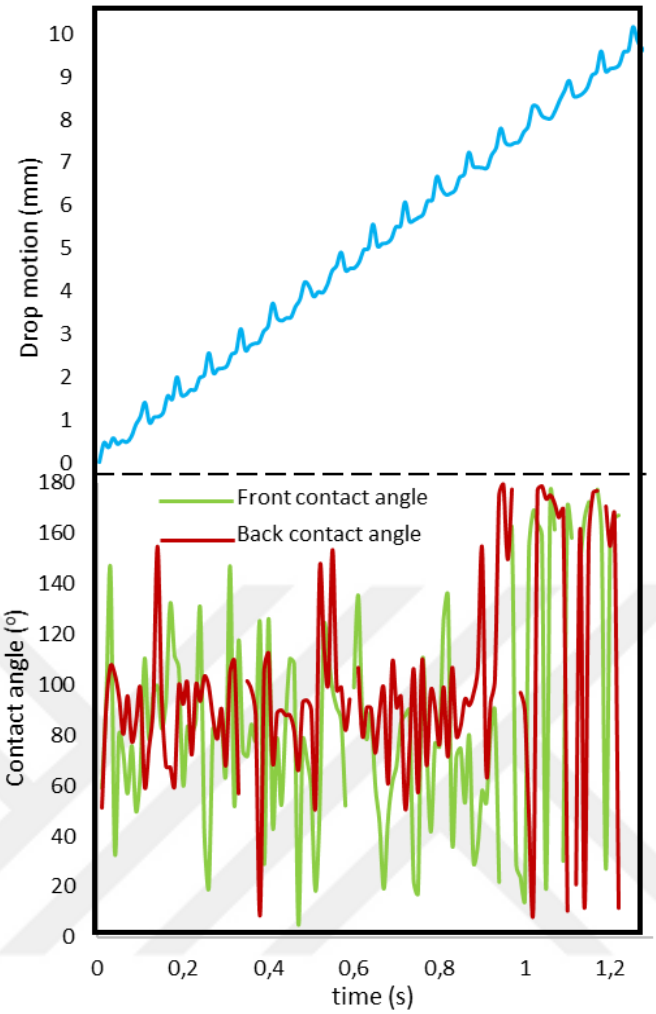

Figure 3. 7. Results obtained from the image processing of hexadecane droplet transportation video. Top image shows droplet position versus time and bottom image shows front and back contact angles of the droplet versus time on the textured ratchet track of 50 µm (1.6) at 43Hz and 8.8g.

In order to understand the effect of the track design on transport dynamics, movement of hexadecane droplets on the tracks with 50 µm (1.2) and 65 µm (1.2) were analyzed and the graphs obtained were shown in the Figure 3.8. and Figure 3.9.

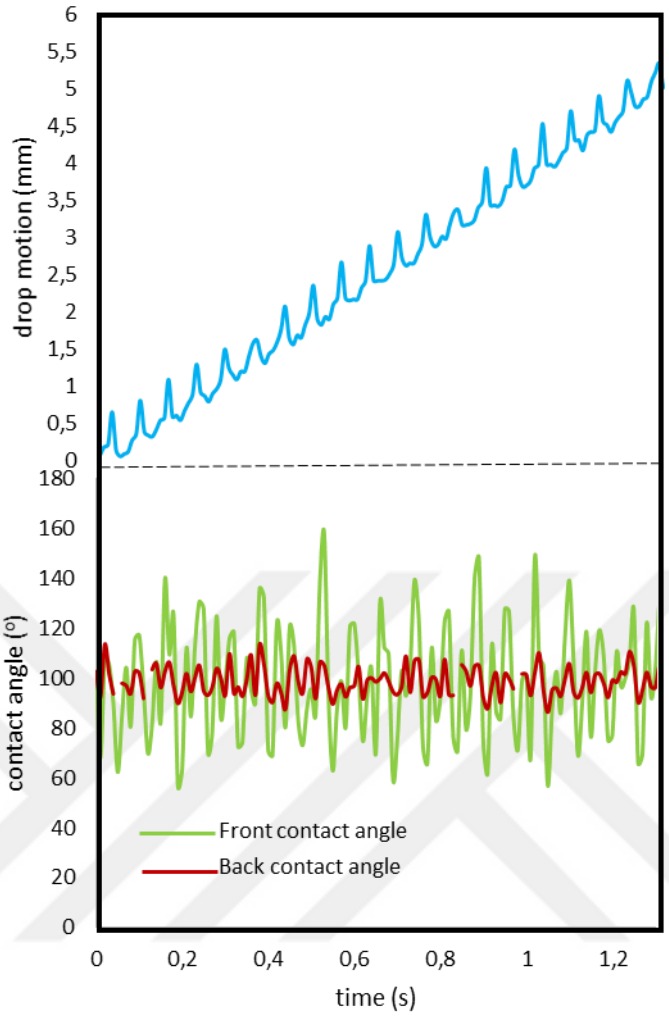

Figure 3. 8. Results obtained from the image processing of hexadecane droplet transportation video. Top image shows droplet position versus time and bottom image shows front and back contact angles of the droplet versus time on the textured ratchet track of 50 µm (1.2) at 43 Hz and 8.8 g.

Hexadecane droplet (4µL) moved on the ratchet track of 50 µm (1.2) at the same frequency, 43 Hz, and threshold value of the acceleration, 8.8 g. However, droplet this time has a lower velocity than the one moves on the track of 50 µm (1.6). The velocity of the droplet was measured as 3.7 mm/s.

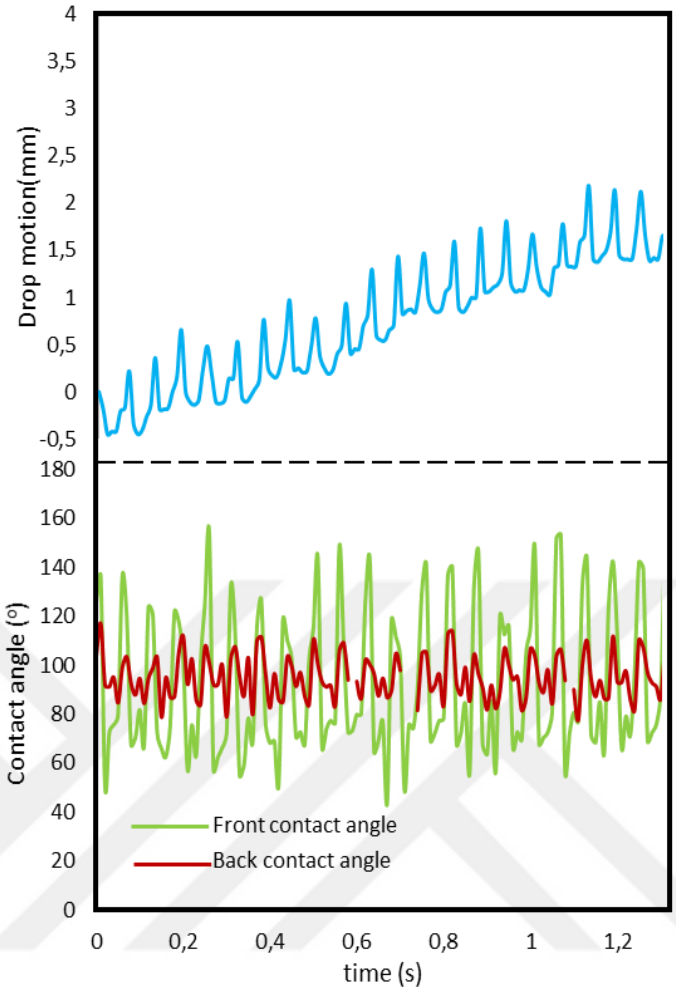

Figure 3. 9. Results obtained from the image processing of hexadecane droplet transportation video. Top image shows droplet position versus time and bottom image shows front and back contact angles of the droplet versus time on the textured ratchet track of 65 µm (1.2) at 43Hz and 10.2 g.

Hexadecane droplet (4µL) moved at the ratchet track of 65 µm (1.2) at the same frequency,43Hz, however, the threshold value of the acceleration was 10.2 g which was higher than the ones on the track of 50 µm (1.2) and 50 µm (1.6). However, the droplet moves in the long distance at 43 Hz and 10.2 g. Consequently, the image processing was performed for the droplet movement on 65 µm (1.2) at 43Hz and 10.2 g as in Figure 3.9. According to the droplet location versus time graph, comparing with the other two tracks, droplet has lowest velocity with the 1.41 mm/s value. Table 3.2. shows the velocities of the

hexadecane droplets on the different racthet designs experimented at the same frequency.

Table 3. 2. Average velocity of the hexadecane droplets on the different ratchet tracks at same frequency

Ratchet Tracks	Average Velocity (mm/s)
50 µm (1.6)	8.13
50 µm (1.2)	3.72
65 µm (1.2)	1.41

The mapping of the frequency and threshold value of acceleration combinations where the droplet is able to move was shown for the three different tracks: 50 µm (1.6), 50 µm (1.2) and 65 µm (1.2) as in Figure 3.10. The threshold of acceleration was found by rising the accelation from 0 g at a frequency set between 15 - 65 Hz. According to the graph, hexadecane droplets (4 µL) moved only between 20 and 60 Hz . When the frequency was lower than 20 Hz or higher than 60 Hz, it went off the track. It is also important to note that the range of frequency and accelaration combinations at which droplets move were similar in all tracks.

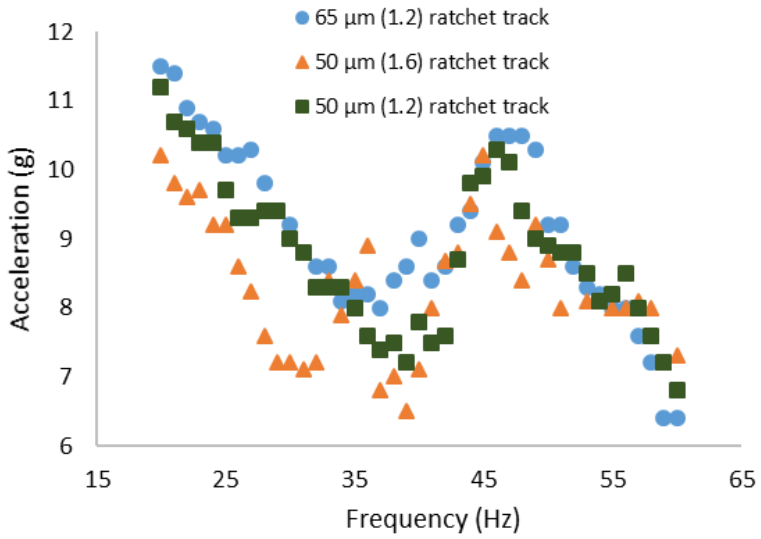

Figure 3. 10. Mapping of frequency and amplitude. Data for 50 µm (1.6), 50 µm (1.2) and 65 µm (1.2) ratchet tracks.

The frequency and acceleration combination at which the droplet can be transported depends on the viscosity and volume of the droplet[3, 4]. Therefore, in order to observe the effect of volume; hexadecane droplets with a volume of 3 µL, 4 µL and 5 µL were moved on the 65 µm (1.2) ratchet track and combination of acceleration and frequency was recorded. Figure 3.11. shows the mapping of the threshold value of acceleration and frequency for different volumes of hexadecane droplets. As the volume decreases, the threshold value of acceleration increases, and the graphs shift toward up. Thus, since the threshold acceleration is different for the different volumes of droplets, droplets can be transported selectively. It is an important feature for controlling the different droplets simultaneously, which was also used for nanoparticle synthesis in Bastopcu et al.'s work [4].

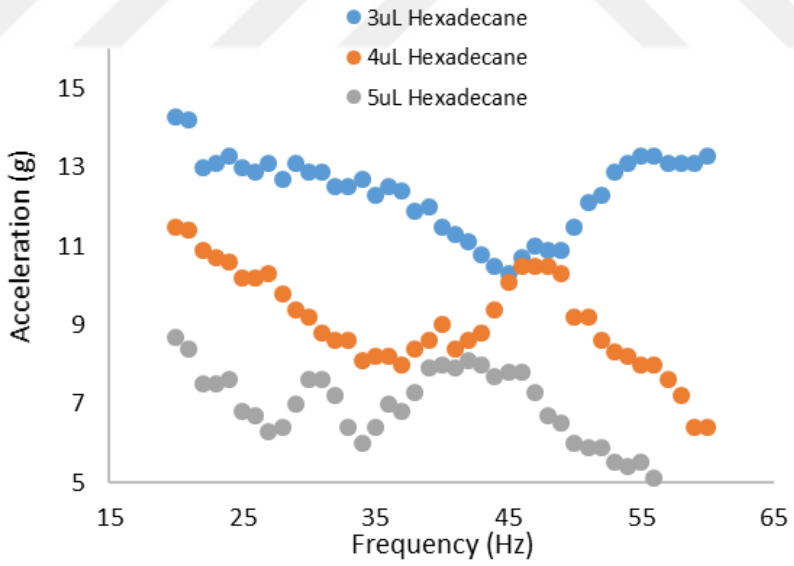

Figure 3. 11. Mapping of frequency and amplitude. Data for 3µL, 4µL and 5µL hexadecane droplet transported on 65 µm (1.2) ratchet tracks.

3.5. Conclusion

In summary, superomniphobic textured ratchet tracks for the oil droplet transportation was developed and experimented. These surfaces were composed of arc shaped arrays; their width and the space ratio were designed based on the experimental results of textured surfaces without energy gradients explained in Chapter 2. In addition to that, mushroom microstructures were used in order to achieve the superoleophobicity. Accordingly, textured ratchet surfaces were fabricated by using the same fabrication steps explained in Chapter 2. Later, these fabricated ratchet tracks were tested for hexadecane, olive oil and coconut oil droplet transportation. While all the fabricated textured ratchet surfaces maintained the transportation for hexadecane droplets, none of them was able to transport the olive oil and coconut oil droplets. At the final stage of the experiment, the best three tracks on which the droplet transported continually in the longest distance were selected as 50 µm (1.6), 50 µm (1.2) and 65 µm (1.2). The videos of the hexadecane droplet movement on the best three tracks at the same frequency were recorded by the high speed camera and the dynamics of the transportation were compared with each other by the image processing software system. Consequently, the highest velocity of the hexadecane droplet was found as 8.13 mm/s and the lowest was found as 1.41 mm/s. In addition, the driving acceleration and frequency of the vibration at which droplet starts to move were recorded for the hexadecane droplet (4 µL) on the three ratchet tracks with different designs. Finally, volume effect on the control parameters (frequency and acceleration) were observed by finding the frequency and acceleration combinations for droplets with 3 µL, 4 µL and 5 µL volume on the same ratchet track design.

3.6. Notes to Chapter 3

1. Shastry A, Case MJ, Bo KF. Directing Droplets Using Microstructured Surfaces †. 2006;(6):6161-6167. doi:10.1021/la0601657

2. Shastry A, Taylor D, Böhringer KF. Micro-structured surface ratchets for droplet transport. TRANSDUCERS EUROSENSORS ’07 - 4th Int Conf Solid-State Sensors, Actuators Microsystems. 2007;(July):1353-1356. doi:10.1109/SENSOR.2007.4300393

3. Duncombe TA, Erdem EY, Shastry A, Baskaran R, Böhringer KF. Controlling liquid drops with texture ratchets. Adv Mater. 2012;24(12):1545-1550. doi:10.1002/adma.201104446

4. Baştopçu M, Derinöz AE, Yilmaz AC, Erdem EY. Textured surfaces as a new platform for nanoparticle synthesis. Soft Matter. 2018;14(21):4311-4316. doi:10.1039/c8sm00091c

Chapter 4

OIL BASED NANOPARTICLE SYNTHESIS ON SUPEROMNIPHOBIC SURFACES

Synthesizing nanoparticles with microfluidic systems is advantageous due to the increased control over reaction parameters. In order to have uniformly distributed narrow-size particles, the mixing ratios, reaction time and temperature should be controlled precisely[2]. Conventional bulk synthesis has some problems in controlling these parameters such as uneven mixing, temperature variations, excessive reaction times. On the other hand, microfluidic systems are better at controlling these parameters and they are also advantageous in scaling up and reproducibility[3, 4]. Therefore, in the last two decades, microfluidic devices have been preferred for nanoparticle synthesis over conventional bulk synthesis. However, among the microfluidic systems mostly closed channel microfluidics was used[5] and the usage of the surface based microfluidic systems have remained limited.

Nanoparticle synthesis in channels has some limitations such as channel clogging, cross-contamination, difficulty in the flow control in the channel. Surface based microfluidic systems overcome these problems and enable them to collect the sample easily, to perform mixing easily, to control the temperature and to place the resulting nanoparticles at the desired position on the surface[6].

In the literature, water based nanoparticle synthesis was carried out by using a similar surface based microfluidic system[6], however, there isn't any previous research focusing on oil based nanoparticle synthesis. Bastopcu et al. showed gold and iron oxide nanoparticle synthesis on textured ratchet tracks. In their work, they used "T" and "Y" shaped ratchet tracks and aqueous reagents were transported first separately then merged and mixed at the junction. Nanoparticles were formed inside the droplets after merging[6]. This work focused on only water based synthesis. In this thesis, an oil based gold nanoparticle synthesis was demonstrated. For gold nanoparticle synthesis, edible coconut oil was used as in the Kumari et al.'s work. This method is environmentally safe, low-cost and rapid[7]. For this synthesis, two solutions were prepared, and they placed at the edge of each sidetracks with the aim of merging on the middle track.

4.1. Fabrication and Design

In this work, for the synthesis of nanoparticles, "T" shape ratchet track design was used, as the one in Bastopcu et al.'s work[6]. However, the dimensions were designed according to the experimental studies of droplets with low surface tension explained in Chapter 2 and 3. "T" shaped ratchet tracks for the nanoparticle synthesis and the corresponding photomask its fabrication are shown in Figure 4.1. There are three different ratchet track designs with different space ratio and radius of curvature. In all these designs, arcs had a width of 50 µm and side tracks were 900 µm in radius of curvature (RoC). For the two designs, two side tracks merge into middle track with same dimensions and same width of 1.6mm, (50 1.2 µm 900 RoC, 50 1.6 µm 900 RoC). For the one design, two side tracks merges into a larger track with 1000 RoC and 1.8mm width, (50 1.6 µm 1000 RoC). For each design, side and middle tracks has 1.5 cm length.

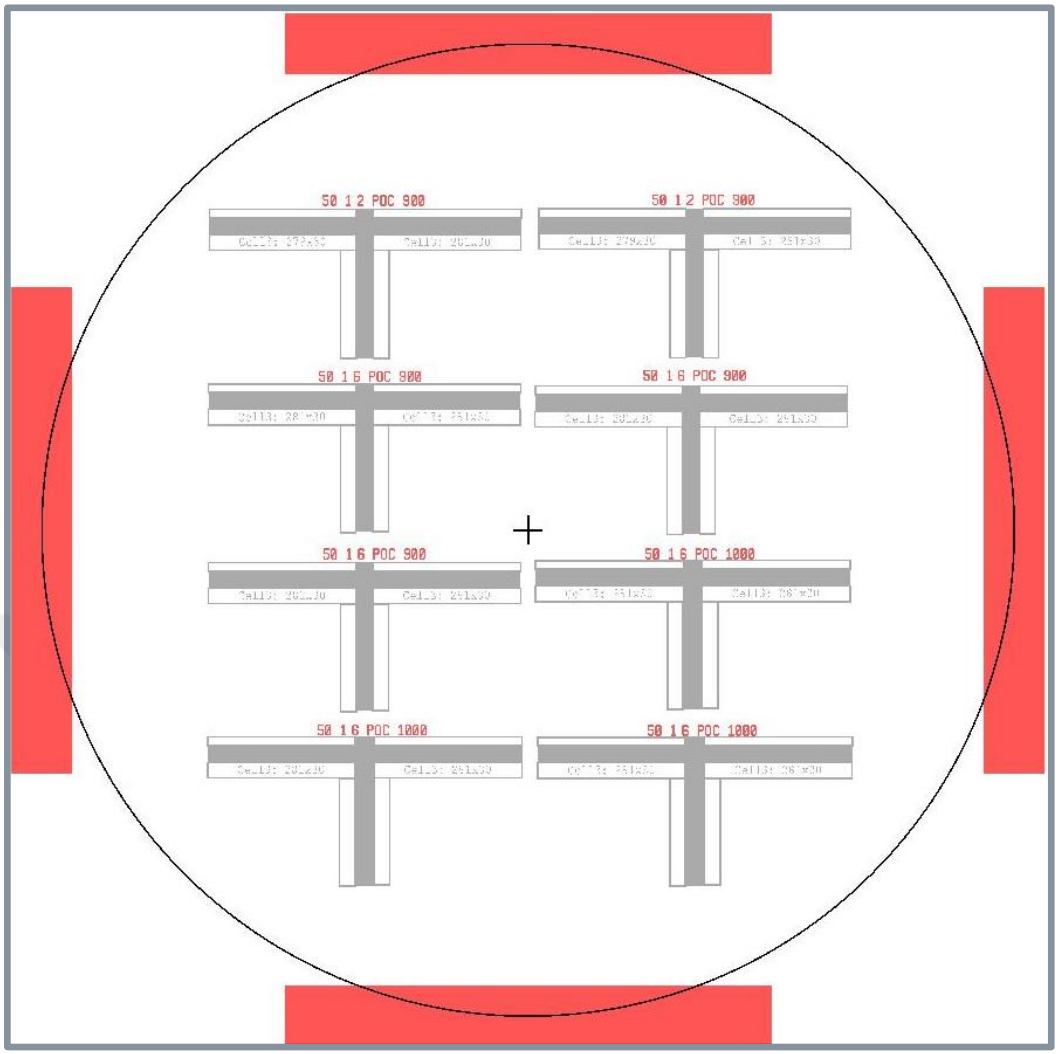

Figure 4. 1. The photomask of textured surfaces for nanoparticle synthesis

Table 4. 1. Textured surface designs with different arc with, space ratio, radius of curvature of the side tracks and middle track

Design#	Arc width (µm)	Space ratio	RoC of side tracks (µm)	RoC of middle track (µm)
1	50	1.2	900	900
2	50	1.6	900	900
3	50	1.6	900	1000

The radius of curvature is important since the droplet should be pinned on the front arc in order to be transported on the ratchet track. According to the experimental studies of the hexadecane droplet movement, it was concluded that

the RoC with 900 µm was suitable for the low surface tension liquid transportation. Thus, mostly 900 µm for the RoC was used. In addition, for one design, 1000 RoC was used for the middle track in order to be able to test nanoparticle synthesis in larger volumes.

According to the Bastopcu et al.'s study, they concluded that T-junction in which the sidetrack has a gap with the middle track gave the better results in merging the droplets than the T-junction in which sidetrack intersects with the middle track[6]. Therefore, in the design, 50-70 µm gap was used between the side and middle track.

4.2. Experimental Methods

Ratchet tracks were fabricated by the conventional lithography method, using the same fabrication process shown in Chapter 2. Mushroom profiled microstructures were used in order to have the oil droplets in Fakir State.

For the Au nanoparticle synthesis, Kumari et al.'s method by using edible coconut oil was followed[7]. Firstly, two reagent solutions, one water based and one oil based, were prepared. First solution was prepared as aqueous solution of HAuCl4 (5.88 * 10-4 M) by using Chloroauric acid (99%) (purchased from the Acros Organics) and distilled water. Here, HAuCl4 solution was used as the source of Au^{+3}. A stock solution was prepared by using high purity coconut oil and acetone with a 1:1 volume ratio. Here, coconut oil was used as a reducing agent, which is non-toxic material unlike the other reducing agents such as NaBH4, citric acid, hydrazine. Acetone was used in order to ease the mixing of water and oil.

The experimental set up which is presented in Chapter 3 was also used for this experiment. Drops with a volume of 3, 4 and 5 µL were taken from the stock solution (acetone and coconut oil) and $HAuCl_4$ solution (5.88 * 10-4 M), later they were placed on both ends of the side surfaces as in Figure 4.2. For the synthesis reaction to take place, HAuCl4 water-based solution was heated to 100^{o}C before placing it on the surface. The stock solution was kept at room temperature. After

the droplets were merged on the ratchet track surface, they were subjected to the vibration with high acceleration for almost one minute in order to be mixed properly. Later the formed droplet together with the surface was placed on the hot plate at 100°C for almost three minutes. Finally, forming nanoparticles as droplets were collected inside a tube.

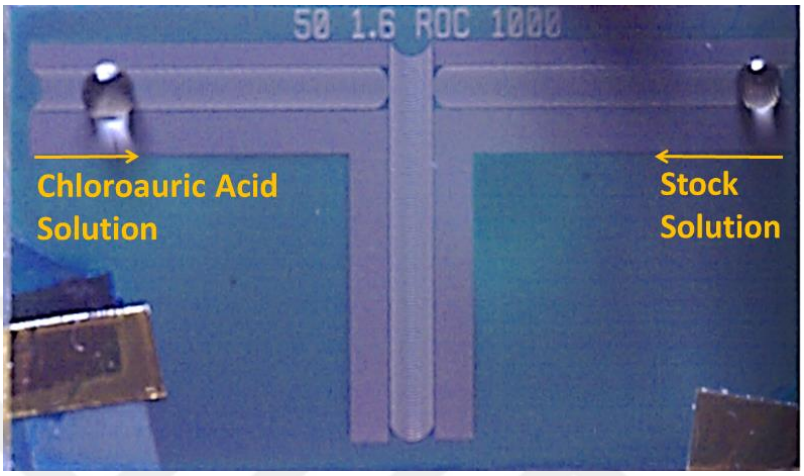

Figure 4. 2. 5 µL Water based $HAuCl_4$ solution placed on the left, 4 µL oil based stock solution placed on the right side of the "T" shaped ratchet track (with 50 µm arc width, 1.6 space ratio, 1000 µm radius of curvature)

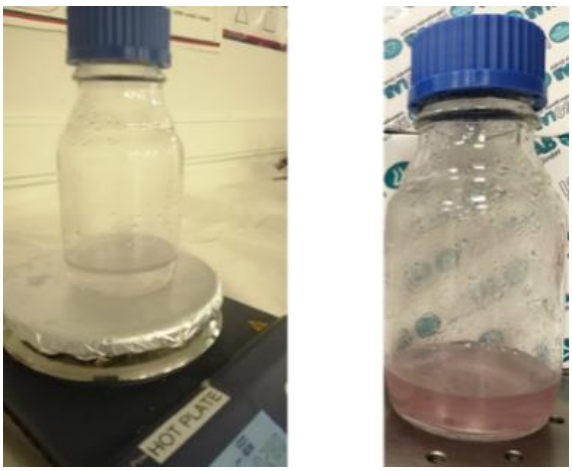

a) b)

Figure 4. 3. a)30 mL $HAuCl_4$ solution and 10 mL stock solution were heating and mixing b) color change of the mixture indicates the gold nanoparticle formation.

The study of Au nanoparticle synthesis was also performed as a conventional batch synthesis. For synthesis, the method of Kumari et al.[7] was applied exactly. First, 30 mL HAuCl4 (2.94 * 10-4 M) solution was heated on the hot plate until it reached 100^{o}C. Then, 10 mL of stock solution (acetone and coconut oil in a 1: 1 ratio) was added into it. The mixture was mixed with a fish magnet on the heater and the color change to the light pink was observed shortly afterward as in Figure 4.3.

For the characterization of nanoparticles synthesized on ratchet tracks, Transmission Electron Microscope and Energy Dispersive X-ray Spectroscopy were used. Samples were prepared with the help of drop casting method after the synthesis droplet was dried on the platform. For the characterization of nanoparticles synthesized by conventional batch wise method, UV-Visible Light Spectroscopy was used.

4.3. Results and Discussion

Droplets of each solution were placed on the side tracks and vibration was applied. Since one of the reagents is water ($HAuCl_4$ solution) and the other is oil (stock solution) based, there is a significant difference in their surface tension. Therefore, their contact line oscillations were different from each other. While water based solution can move at the lower acceleration, for the oil-based solution, much higher acceleration was required. For instance, between 30 Hz and 40 Hz frequency, water based solution moved at 8 -15 g, whereas oil based solution moved at 15 -25 g.

In addition, the fabricated “T” shape ratchet tracks were not able to transfer the stock solution from the side track to the middle track. It was spreading on the junction point as in Figure 4.4. As it is clear from the image, $HAuCl_4$ water-based solution could not follow the track at 34 Hz and 10 g and jump out from it. This problem was still observed even at different frequency and acceleration matching. The reason for this is that the surface is very repulsive for water and therefore the water makes 180° CA.

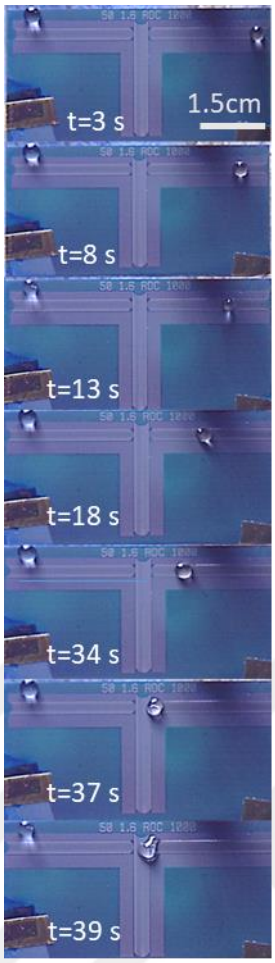

Figure 4. 4. Movement of 5 µL $HAuCl_4$ solution and 4 µL stock solution at the 34 Hz and 10 g -15 g on the side tracks (with 50 µm arc width, 1.6 space ratio, 1000 µm Radius of Curvature)

Since the tracks are highly oleophobic, droplet makes little contact with the surface at the front and back, controlling its movement becomes difficult and even at the very small acceleration, it can jump on the surface without following the track. The surface energy of the silicon plate coated with C_4F_8 (~ 11mN / m) is too low for the water droplet.

When the acceleration increased to 15 g, the oil-based stock solution initiated its movement on the side track however when it comes to the end of the track, it could not pass to the middle track and spread at the junction point. This problem, which has been observed for all of the other ratchet track surfaces, could be caused by the low surface energy of the oil.

In the other part of the experimental study, sidetracks were not used and synthesis studies were performed on the middle track by placing droplets one after another in the same track as in Figure 4.5.

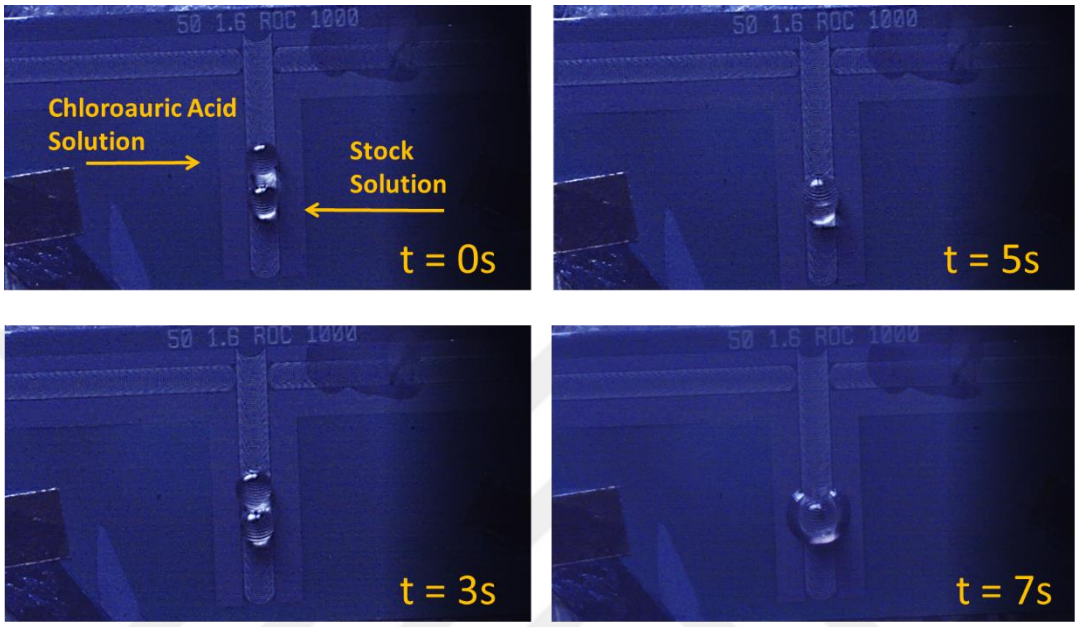

Figure 4. 5. Movement of 4.5 µL $HAuCl_4$ solution and 4.5 µL stock solution at 38 Hz and 8.8 g on the middle track (with 50 µm arc width, 1.6 space ratio, 1000 µm Radius of Curvature)

At the low acceleration, as the water based solution was moving along the track, it merged with the oil based solution in front of it and formed a larger droplet. Resulting droplet pinned and spread on the surface instead of moving along the track. In order to perform required mixing for nanoparticle synthesis, the platform was vibrated at the 12 g for one minute and then was heated on the hot plate at 100^{o}C for three minutes. After mixing and heating, nanoparticles synthesized inside of the resulting droplet and consequently dark colored particles were observed. Finally, nanoparticles were collected inside a tube. The synthesis was performed repeatedly by merging droplets with 1:1 volume ratios until the total volume of the droplet formed is 0.5 mL.

In order to characterize the nanoparticles via Transmission Electron Microscopy, the sample was centrifuged at 13,000 rpm for 15 minutes and washed though the distilled water. In addition, tracks were observed under the Scanning Electron Microscopy (The Quanta 200 FEG ESEM). After the nanoparticles were synthesized on the platform, resulting droplet was dried by using the drop casting method in the air environment and then their SEM image was taken as in Figure 4.6. For their chemical characterization, Energy Dispersive X-ray Spectroscopy (EDX) was used.

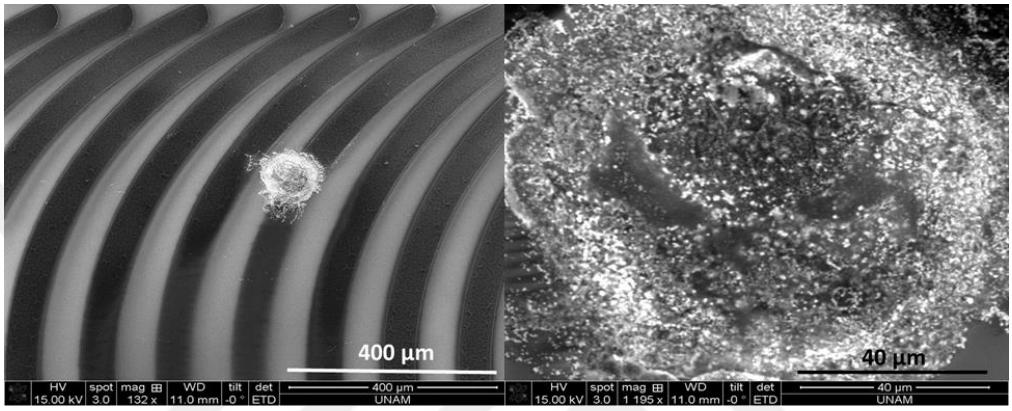

a) b)

Figure 4. 6. SEM images of Au nanoparticle synthesized on the ratchet track a) at 132× magnification b) at 1195× magnification

As shown in Figure 4.6a., white colloid was visible at the 132× magnification mainly corresponds to the Au particle according to the EDX analysis (Figure4.7). According to the EDX result, the image taken at low magnification shows the gold peak clearly with 0.84 atomic percentage. When the surface was observed at higher magnification, 1,195×, white dots were visible and the peak of Au was higher with 3.17 atomic percentage according to the EDX analysis.

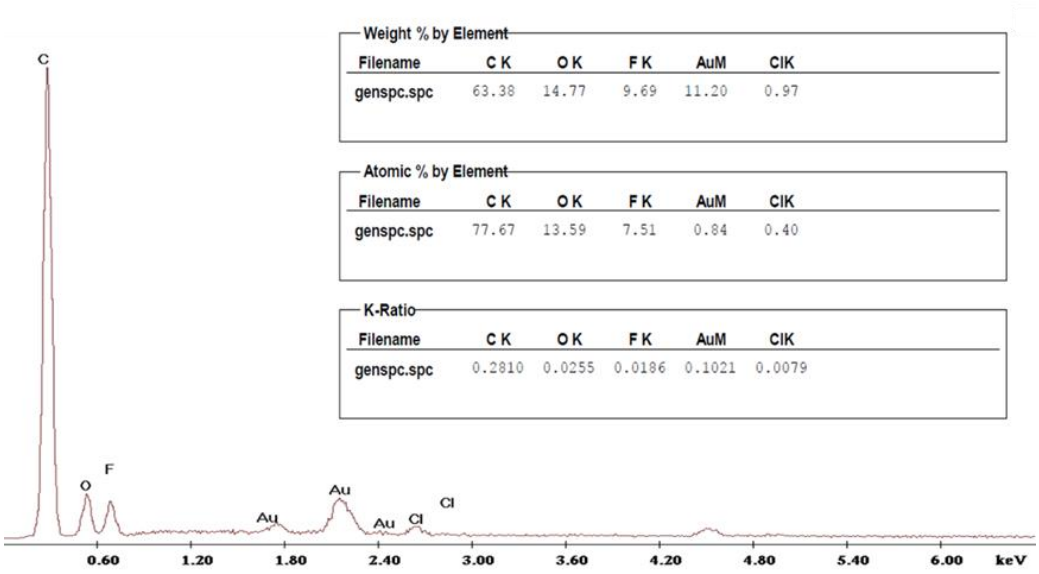

Figure 4. 7. EDX spectrum of Au nanoparticle synthesized on the ratchet track

Nanoparticles (NP) synthesized via batch wise were characterized by using UV-Visible Spectroscopy (Cary 5000-UV-Vis-NIR) at a resolution of 0.8 nm with a scanning speed of 480 nm/min. Figure 4.8. shows the UV-Visible absorption spectra of the sample and as it is clear from the graph, there is a peak at the 556 nm

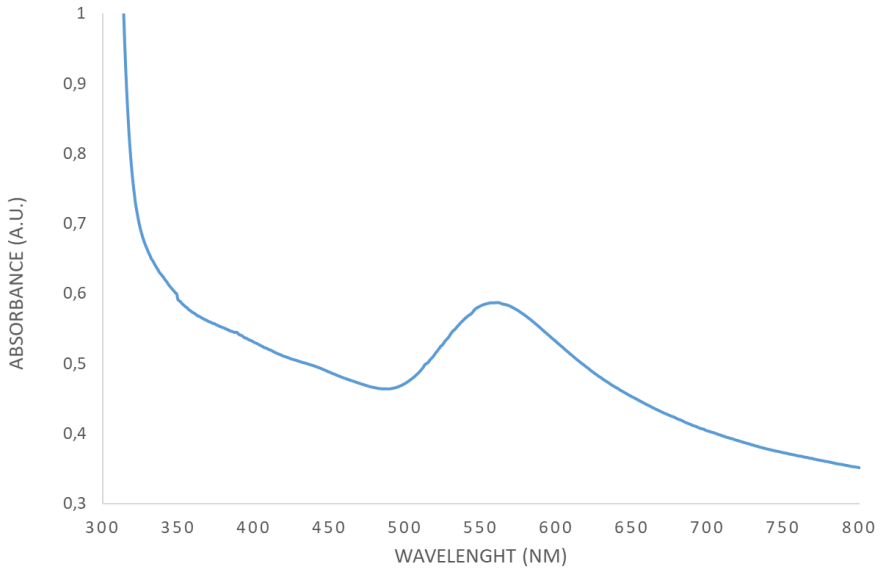

.

Figure 4. 8. UV-Visible spectra of the gold nanoparticles synthesized as conventional batch wise method

This peak corresponds to the gold since the surface plasmon resonance (SPR) band of nanoparticle in the range of 515-572 nm[8]. As the gold particle size increased, their optical properties differentiate and they have broaden SPR peaks and shifts to the longer wavelength. For instance, as the gold NP with 30 nm size has a peak at 526 nm, the one with 60 nm size has a peak at 540 nm. As for the sample that has a peak at 556 nm corresponds to the 80-100 nm size[8].

For the further analysis, centrifuged and washed samples from the platform synthesis and conventional batch synthesis were dried for the X-Ray Diffraction (XRD) analysis. Samples were examined with the help of XPERT-PRO PANalytical device at 45 kV and 40 mA. Analysis results of gold nanoparticles synthesized on the platform (Figure 4.9.) and gold nanoparticles synthesized with batch method (Figure 4.10.) showed that both sample has the peaks of gold nanoparticles nearly at 38.2°, 44.5°, 64.8°, 77.5° and 82.5° respectively from the planes of (111), (200), (220), (311) and (222). The intensity of these peaks were the same as the reference data of the gold nanoparticles (JCPDS No: 04-0784). The formation of gold nanoparticles was justified by the XRD result.

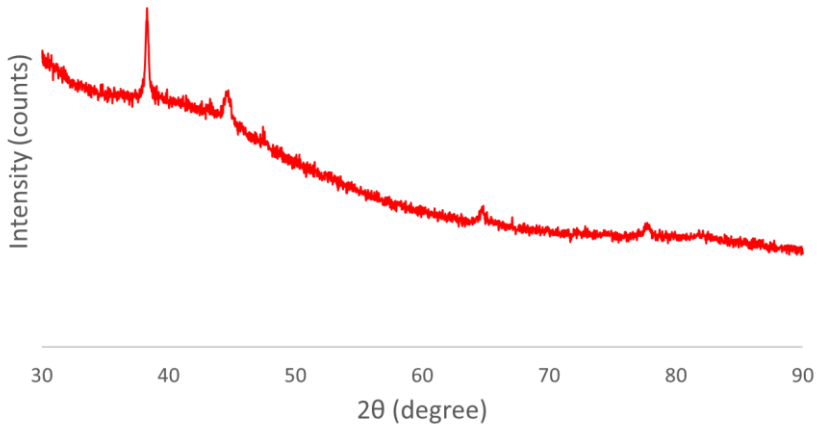

Figure 4. 9. XRD analysis of gold nanoparticles synthesized on the platform

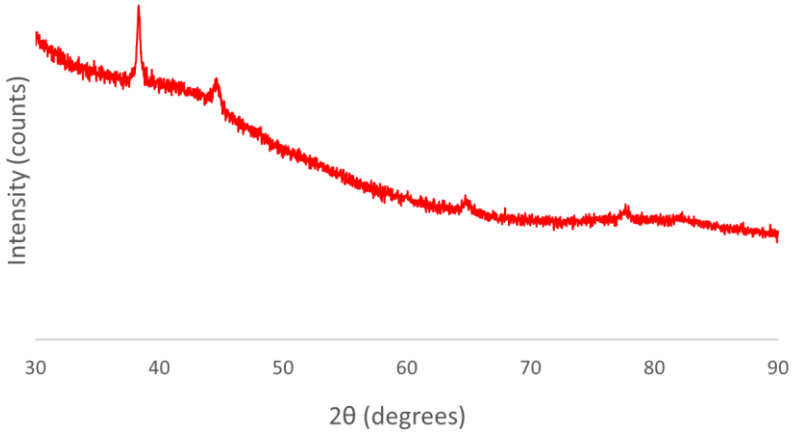

Figure 4. 10. XRD analysis of gold nanoparticles synthesized with the batch method.

In order to compare the size and morphology of the nanoparticles synthesized on the platform and nanoparticles synthesized with the batch method, Transmission Electron Microscopy (TEM) measurements of the samples were performed. TEM images shown nanoparticles synthesized on the platform were not uniform in terms of size and shape (Figure 4.11). These nanoparticles were in the shape of spheroid, triangular, hexagonal and pentagonal shapes. On the other hand, gold nanoparticles synthesized with the batch method were more uniform than the one synthesized on the platform in terms of size (Figure 4.12).

The main reason for the non-uniformity of the platform synthesis can be the temperature control. However, this study achieved to prove the concept of oil based nanoparticle synthesis on the superomniphobic textured ratchet tracks with the help of vibration.

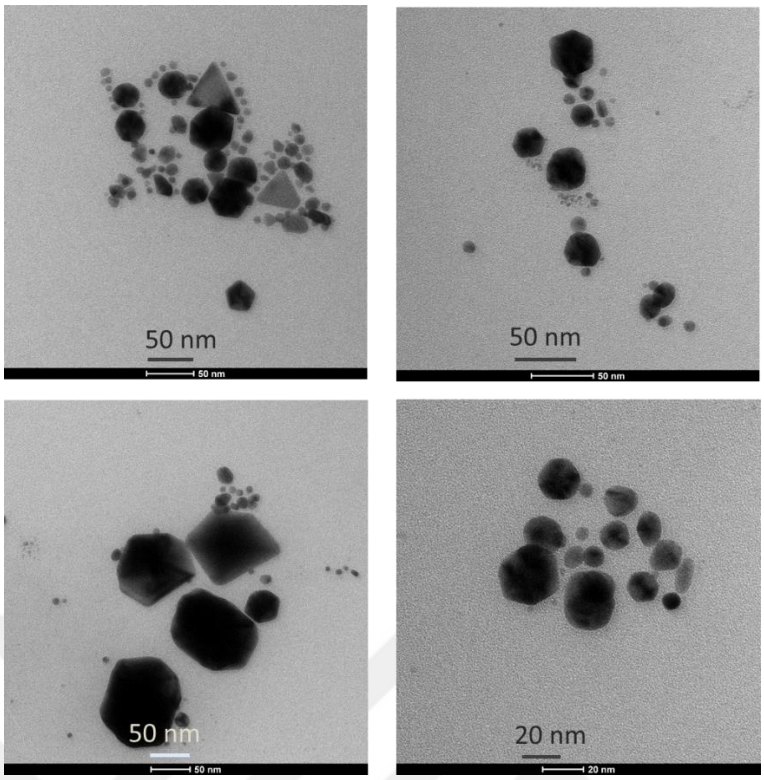

Figure 4. 11. TEM images of gold nanoparticles synthesized on the platform

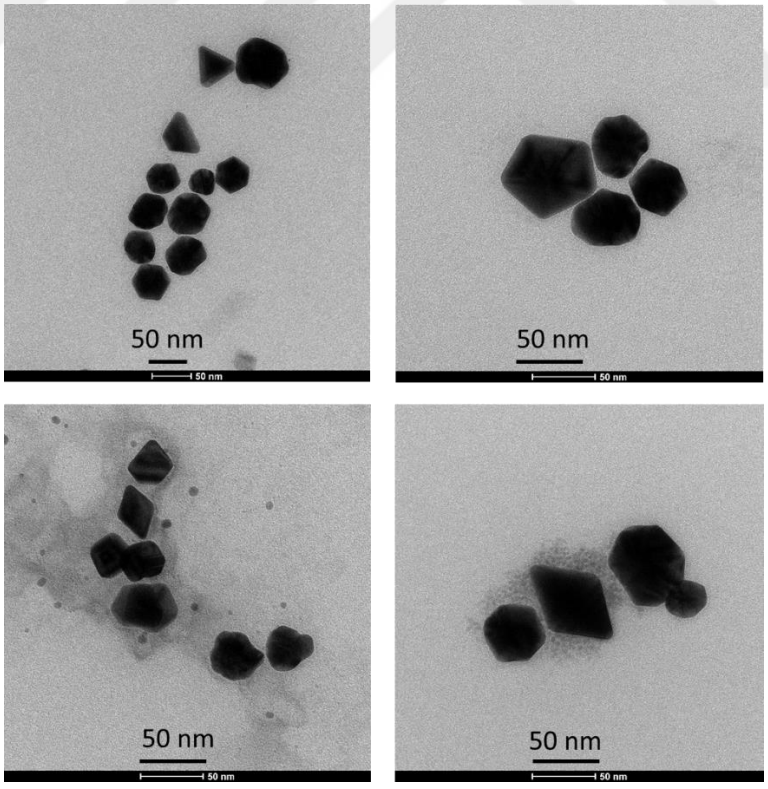

Figure 4. 12. TEM images of the gold nanoparticles synthesized with batch method

4.4. Conclusion

In summary, oil based gold nanoparticle synthesis on the surface based microfluidic platform was reported. First, “T” shape ratchet tracks were fabricated with mushroom microstructure on silicon surface by conventional lithography method. Then, reagents were prepared for gold nanoparticle synthesis with the use of edible coconut oil by following the method of Kumari et al.[91]. The droplet of these reagents were placed on the side tracks of the T shape ratchet tracks and tried to be merged on the middle track at the driving frequency and acceleration matching. However, due to the significant difference in the surface tension of reagents and, consequently, the difference in their contact line oscillations, at high accelerations where the oil-based reagent could be carried, the water-based reagent easily went off the track. Therefore, reagents were placed one after another on the same track and they merged at low acceleration, consequently nanoparticle synthesis took place inside of the droplet. For the characterization of the resulting particle, EDX and XRD were used and the formation of gold nanoparticle was justified. In addition, oil based nanoparticle also synthesized by conventional batch wise method and samples were characterized by using UV-Visible Spectroscopy and XRD. Finally, TEM measurements of both samples were performed to observe their size and morphology.

4.5. Notes to Chapter 4

1. Besson C, Finney EE, Finke RG. A mechanism for transition-metal nanoparticle self-assembly. J Am Chem Soc. 2005;127(22):8179-8184. doi:10.1021/ja0504439
2. Jahn A, Reiner JE, Vreeland WN, DeVoe DL, Locascio LE, Gaitan M. Preparation of nanoparticles by continuous-flow microfluidics. J Nanoparticle Res. 2008;10(6):925-934. doi:10.1007/s11051-007-9340-5
3. PM V, OC F, R K, R. L. Microfluidic technologies for accelerating the clinical translation of nanoparticles. Nat Nanotechnol. 2013;185(2):974-981. doi:10.1038/mp.2011.182.doi
4. Liu Z, Fontana F, Python A, Hirvonen JT, Santos HA. Microfluidics for Production of Particles: Mechanism, Methodology, and Applications. Small. 2019;1904673:1-24. doi:10.1002/smll.201904673
5. Erdem EY, Cheng JC, Doyle FM, Pisano AP. communications Increased Temperature Control in Nanoparticle Synthesis. 2014;(6):1076-1080. doi:10.1002/smll.201302379
6. Baştopçu M, Derinöz AE, Yilmaz AC, Erdem EY. Textured surfaces as a new platform for nanoparticle synthesis. Soft Matter. 2018;14(21):4311-4316. doi:10.1039/c8sm00091c
7. Meena Kumari M, Philip D. Facile one-pot synthesis of gold and silver nanocatalysts using edible coconut oil. Spectrochim Acta - Part A Mol Biomol Spectrosc. 2013;111:154-160. doi:10.1016/j.saa.2013.03.076
8. Gold nanoparticles: Properties and applications. (n.d.). Sigma-Aldrich. https://www.sigmaaldrich.com/technicaldocuments/articles/materials-science/nanomaterials/gold-nanoparticles.html

Chapter 5

CONCLUSION AND FUTURE OUTLOOK

The objectives of this research thesis were to transport of the oil droplet on the superomniphobic textured ratchet tracks and to perform oil based nanoparticle synthesis on these surfaces. To achieve these goals, first superomniphobic textured surfaces with two different microstructures were developed: mushroom and straight sided microstructures. In addition, the effect of topography to the oleophobicity was investigated. According to the characterization results, it was concluded that mushroom microstructure is the key parameter for superoleophobicity. Thereafter, best superoleophobic surfaces were selected according to the contact angle measurement results of hexadecane and their geometrical ratios were implemented to the superoleophobic textured ratchet tracks. For the fabrication of the textured ratchet tracks, mushroom profile was used to maintain superoleophobicity. Further, fabricated ratchet tracks were tested for hexadecane, coconut oil and olive oil droplets and hexadecane droplet transportation on these surfaces was reported. According to the length of the path the droplet takes, best three track were selected as 50 µm (1.6), 50 µm (1.2) and 65 µm (1.2). The transportation of hexadecane droplet on these tracks were extensively studied by modelling its movement and examining its dynamics. Their velocities were found as 8.13 mm/s, 3.72 mm/s and 1.41 mm/s. This project is the first study shows the continuous and controlled transportation of oil droplet in the ambient air. The mapping of threshold value of acceleration and frequency where the hexadecane droplet initiate the movement was shown for best tracks as 50 µm (1.6), 50 µm (1.2) and 65 µm (1.2). Besides, volume effect of the droplets on the droplet dynamics (frequency and acceleration combinations) were studied by obtaining the mapping of frequency and acceleration combinations for the three different volume of hexadecane droplet. At last, we demonstrated oil based gold

nanoparticle synthesis on these surfaces. For the nanoparticle synthesis, “T” shape ratchet tracks were designed, their dimensions were selected among the dimensions of the best ratchet tracks (50 µm (1.6), 50 µm (1.2)). For the oil based nanoparticle synthesis, two different reagent were prepared as oil based and water based. Oil based reagent consisted of edible coconut oil and acetone, water based reagent consisted of $HAuCl_4$ aqueous solution. The droplet of reagents were placed at the each end of the side track and expected to merge with each other in the middle track. However, due to their surface tension difference, they could not be transported at the same frequency and acceleration and the track was too repellent for the water based reagent so that it went off the track. Therefore, reagents were merged on the middle track by placing one after another at the middle track. Resulting nanoparticle was characterized by the SEM-EDX and XRD and gold peak was clearly observed.

In this thesis, only two types of design were used: straight path for the oil transportation and “T” junction path for nanoparticle synthesis. However, the paths can be designed differently and can be carried to the desired location according to the purpose of the application. For example, by the closed circular path, it can have a longer path in order to have longer mixing function for nanoparticle synthesis or it can be designed with a wider path in order to transport reagents with larger volumes. In addition, its ability to transport the low surface tension liquids opens up possibilities for microfluidic systems for performing biochemical and chemical reactions since many biological and chemical samples have low surface tension. Furthermore, this platform can be used for smart surfaces in moving vehicles, with a natural vibration, requires self-cleaning or oil repellency.

Overall, this platform is able to move oil based droplets by only using one input (vibration), it can be used many times without the loss of performance, it does not require any pump or tubing, and it is simple, cost effective and flexible. Moreover, since it is chemically and thermally stable, there is no undesirable side effects for the biological and chemical reactions.